A Study on the Development and Utilization of a Micro-Endoscopic System for Functional Assessment of Neural Circuits in Deep Brain Regions

by

Hidetaka Yashiro

Doshisha University
Graduate School of Life and Medical Sciences

November 2017

Doshisha University
Graduate School of Life and Medical Sciences

―――――――――――――――――

ABSTRACT

―――――――――――――――――

A Study on the Development and Utilization of a Micro-Endoscopic System for
Functional Assessment of Neural Circuits from Deep Brain Regions

by Hidetaka Yashiro

In vivo imaging has become a powerful tool for examining the relationships among neighboring cortical neurons. Currently, the limitations of this technique are the shallow depth at which good measurements are possible and the low temporal resolution. The aim of this study was the development of a novel micro-endoscopic system that addresses these issues by combining imaging that can be performed at deeper depths with simultaneous electrophysiological recordings of both local field potentials and multiunit activities. Our system, which consists of a micro-endoscope that is coated with gold and is insulated, conducts simultaneous optical imaging and electrical recordings. Thus, this micro-endoscopic system enables us to simultaneously monitor the responses of multiple neurons using the changes in fluorescence of the calcium fluorescent indicator dye, which reflect calcium activation, and electrophysiological recordings (local field potentials and multiunit activities) made with the edge of a fiber electrode. We used this system to record calcium activation occurring in response to sound stimuli at different depths (0–1,500 μm from the dorsal surface) of the inferior colliculus (IC) in mice and two species of bats (*Carollia perspicillata* and *Eptesicus fuscus*). We compared the response profiles to different frequencies across the recording methods and found that our method accurately mapped the dorsoventral tonotopicity of the inferior colliculus. We also compared the optical images of the calcium responses to the auditory stimuli with the simultaneously recorded local field potentials and multiunit activities. These comparisons showed that the calcium responses were slow, occurring in the 70–130 ms range, and the peak latencies of the calcium responses and electrophysiological responses differed significantly. The slow time course of the calcium responses corresponded with the slow inhibitory events that determine response latencies in the inferior colliculus and not the fast time course of the responses that encode the biosonar information.

TABLE OF CONTENTS

LIST OF FIGURES

ACKNOWLEDGEMENTS

CHAPTER 1.

INTRODUCTION

1.1 Optical neural recordings: voltage and calcium imaging

Optical measurements have the advantage of making the simultaneous recording of the activities of multiple neurons possible, unlike electrophysiological recordings. A method for performing optical measurements of membrane potentials was proposed in 1968 (Cohen et al., 1968; Tasaki et al., 1968; Cohen et al., 1969). A voltage-sensitive dye (VSD) that emits fluorescence according to the membrane potential has been developed and used in optical imaging (Peterka et al., 2011). This method enables us to visualize neural activities as changes in fluorescence. In the 1980's, a calcium-sensitive dye (CSD) that converts the intracellular calcium ion concentration into the intensity of fluorescence was developed, and many calcium-imaging experiments using a CSD have been performed (Grienberger and Konnerth, 2012). Although these two methods are very useful for neuroscience research, calcium imaging has been conducted more frequently because CSDs have a greater fluorescence intensity and lower toxicity to cells compared with VSDs (Tsien, 1980, 1981). Currently, the CSDs that are widely used are Oregon Green and Fluo-4, and fluorescent signals with good signal-to-noise ratios are relatively easy to obtain (Paredes et al., 2008). In addition, a calcium-sensitive fluorescent protein has been developed (Miyawaki et al., 1997), and the use of mutant animals with cells that are genetically labeled with a fluorescent protein has recently been reported (Grienberger and

Konnerth, 2012; Looger and Griesbeck, 2012; Bovetti et al., 2014).

1.2 Multiphoton imaging

Although a method for optical neural recording has been developed, as described in the previous section, *in vivo* optical measurements are hampered by limitations in the depth of the recordings that can be made. The measurable thickness that can be made using a confocal microscope is only approximately 50 μm (Sandison and Webb, 1994). A two-photon excitation microscope that was developed in the 1990's (Denk et al., 1990; Nakamura, 1999) made it possible to measure deep brain areas. With this measurement method, the focal depth can be changed arbitrarily, and measurements can be made up to a depth of approximately 800 μm with two-photon imaging and approximately 1,100 μm with three-photon imaging (Helmchen and Denk, 2005; Horton et al., 2013). Currently, several studies have been conducted that combine multiphoton imaging and calcium imaging methods, and these studies have revealed the cortical layer structure (Bovetti et al., 2014).

1.3 The auditory system in mammals

Mammals, including humans, have similar auditory pathways. First, sound waves, which are air vibrations that propagate through the air, reach the cochlea via the tympanic membrane and auditory ossicles (malleus, incus, and stapes). The basilar membrane in the cochlea has a tonotopic structure for neural coding. The sound wave signals are coded

into neuronal electrical signals from the physical signals (Durrant and Lovrinic, 1995a). The information thereafter travels via the auditory nerve (VIII nerve), cochlear nucleus (CN), superior olive complex (SOC), lateral lemniscus (LL), inferior colliculus (IC), and medial geniculate body (MGB) to finally arrive at the auditory cortex (AC) (Durrant and Lovrinic, 1995b). Auditory responses from each auditory station have been reported to correspond to the I–VII waves of the auditory brainstem responses. However, the location of the signal source is unclear except for the I and II waves from the AN and CN, respectively, because the waves remain, even if the corresponding station is ablated (Starr and Hamilton, 1976; Melcher et al., 1996; Melcher and Kiang, 1996; Parkkonen et al., 2009).

1.4 The inferior colliculus

The IC is the largest auditory station in the midbrain. The IC is divided into the following three parts: the dorsal cortex (DC), lateral cortex (LC), and central nucleus (ICC) (Oliver, 2005). The ICC, which is the largest part of the IC, is covered by the DC and LC (Ito and Oliver, 2012). In the afferent pathway, the IC receives ipsilateral projections from the CN, SOC, and LL and contralateral projections from the CN and LL (Cant, 2005; Schofield, 2005). The IC subsequently projects to both sides of the MGB (Wenstrup, 2005). The ICC has a multilayered structure. Each lamina, which consists of projection fibers, neurons, and dendrites, is adapted to respond to a specific frequency. These laminae have high frequency selectivity, which results in tonotopic organization (Stiebler and Ehret, 1985). This tonotopic organization exhibits a dorsoventral multilayered pattern: the dorsally located laminae respond more intensely to lower frequencies, whereas the

ventrally located laminae respond more to higher frequencies (Schreiner and Langner, 1997; Portfors et al., 2011). In addition, neurons that respond specifically to amplitude-modulated sounds and frequency-modulated sweep sounds have been described in the IC (Rees and Møller, 1983). Neurons that change their firing rate according to the sound pressure level (SPL) have also been described in the IC (Rees and Palmer, 1988). Combination-sensitive neurons (CSNs; facilitative neurons), which respond to specific sound combinations to detect differences in the timing of pulses and echo during echolocation (Feng et al., 1978; Suga et al., 1978; O'Neill and Suga, 1979; Sullivan, 1982; Schuller et al., 1991; Fitzpatrick et al., 1993; Wenstrup et al., 2012; Suga, 2015), have been reported in the IC of bats (Feng et al., 1978; Dear and Suga, 1995; Wenstrup et al., 2012; Suga, 2015). The homolog of the lateral cortex of the IC in owls contains an auditory spatial map, which is a neural reproduction of the sound source directions (Knudsen and Konishi, 1978). These findings indicate that various types of neurons are located in the IC and that the IC performs complicated information processing.

1.5 Echolocation

The word echolocation, which is composed of the words *echo* and *location*, is the ability to perform sound localization using information contained in the reflecting echoes. Some mammals, such as bats and whales (including dolphins and porpoises), have this ability. They can fly/swim and chase flies/fish in low-visibility environments (Pierce and Griffin, 1938; Kellogg and Kohler, 1952; Schevill and McBride, 1956; Griffin, 1958). The basic principle of echolocation is the same in these animals. The animals emit an ultrasonic pulse and compare it with the reflecting echoes. Whales emit ultrasonic waves from their

peculiar organ called the "melon," and the echo sounds are detected by their lower jaw, which is connected to their ears. The melon, which mostly consists of fat and adipose tissue, acts as an impedance matcher of the sound transmission and water (Ketten, 1997). In contrast, bats use their vocal cords and mouths or nostrils to emit ultrasonic pulses and then catch the echoes with their ears (Neuweiler, 2000b). Echolocation is innate in these animals. However, it has been suggested that humans can acquire this ability with training (Thaler and Goodale, 2016).

1.6 Echolocating bats

Bats are the second largest order of mammals after rodents, and 71 % (approximately 700 species) are insectivorous, 23 % (approximately 230 species) are frugivorous, 5 % (approximately 50 species) are nectarivorous or pollenivorous, and the rest (1 %, 10 species) are sanguivorous or carnivorous (Neuweiler, 2000a). Insectivorous bats and some neotropical frugivorous bats are echolocating bats that use echolocation to orient and guide their flight in their surroundings (Neuweiler, 2000b). Most species transmit trains of brief frequency-modulated (FM) sounds and then exploit the wide bandwidth of the signals to perceive the objects as acoustically derived images (Simmons, 2012). The distance to the reflecting objects, such as insect prey, is determined by the time delay between the outgoing biosonar broadcasts and the returning echoes, whereas distinguishing features of the object, such as its shape and size, are determined by comparing the echo spectra with the broadcast spectra (Simmons et al., 1995; Simmons, 2012).

1.7 Previous findings related to the current study

Although several multiphoton imaging experiments have been performed (Grienberger and Konnerth, 2012), their results are limited because of the restrictions in the recording depths that can be accessed. Therefore, several studies have suggested that the insertion of optical fiber bundles into the deep areas might be effective in overcoming this limitation (Flusberg et al., 2005; Vincent et al., 2006; Murayama et al., 2007; Rochefort et al., 2008; Grewe and Helmchen, 2009; Murayama and Larkum, 2009; Grienberger et al., 2012; Grienberger and Konnerth, 2012; Hayashi et al., 2012; Schulz et al., 2012; Osanai et al., 2013). These methods make it possible to image neurons in deep brain areas by combining a gradient-index lens or optical fiber bundle with a fluorescent microscope. In addition, the focal depth can be adjusted by attaching an electrowetting variable-focus lens to the tip of the optical fiber bundle (Ozbay et al., 2015). These endoscopic methods enable not only deep brain measurements, but also the ability to conduct optical measurements in freely moving animals (Goto et al., 2015; Hamel et al., 2015; Ziv and Ghosh, 2015; Miyamoto and Murayama, 2016).

1.8 Purpose

The purpose of this study was to establish a method to use to perform simultaneous optical and electrical recordings of auditory responses and activity in deep brain regions. Electrophysiological recordings have revealed the functions and characteristics of the auditory brain areas. However, because almost all auditory brain areas, except for the AC and IC, are located in deep regions of the brain, optical measurements have been difficult

in the auditory areas, and the neural circuits therein have not been clearly described. By establishing a method for the performance of optical measurements in deep brain regions, we will be able to examine the neural circuits underlying auditory neural processing. For example, bats search for objects by comparing the ultrasonic pulses they emit with the echoes that are reflected from the object (Neuweiler, 2000b). This processing occurs in milliseconds (Simmons, 2012), and optical measurements will help elucidate the neural mechanisms that underlie this high-speed neural processing. However, although the spatial resolution of optical measurements is high, its temporal resolution is limited. In order to address these issues, we developed a micro-endoscopic system and used it to optically and electrically measure auditory responses in the IC of mice and bats. In addition, we restricted the scanning area to attempt to improve the temporal resolution. Our aim was to establish a method to use to perform optical and electrical recordings in deep brain areas, and we believe that this method enables us to compare optical auditory responses with electrophysiological responses to reveal neuronal circuits.

1.9 Major Contributions

The major contributions of the work presented in this dissertation are the following:

1. We developed a micro-endoscopic system that can be used to assess the function of neuronal networks in deep brain regions where conventional optical recording systems, such as epi-fluorescent microscopy and multiphoton excitation microscopy, were not useful. This system enabled us to obtain optical images with spatial resolution that was adequate for the detection of individual cell bodies with minimal invasion (Yashiro et al., 2017a).

2. Simultaneous optical and electrical recordings were conducted with the micro-endoscopic system. To record electrical activity, an endoscope tip was coated with gold and enamel and used as an electrode. Auditory responses were subsequently optically and electrically recorded in the IC of mice. We were able to recognize the tonotopic organization of the IC with the optical responses: dorsally located cells responded more intensely to lower frequencies, whereas ventrally located cells responded more to higher frequencies (Yashiro et al., 2017a).

3. Changes in the fluorescence of a calcium fluorescence indicator dye that reflected calcium activation dye were recorded in the IC of two species of FM-echolocating bats (*Eptesicus fuscus* and *Carollia perspicillata*) using our micro-endoscopic system (Yashiro et al., 2017b).

4. The temporal resolution of the optical recordings was not sufficient to allow millisecond observations of neural activity. Our endoscopic time resolution was also slow: approximately 18.9 frames/s (53 ms/frame). We therefore attempted to enhance the resolution by scanning only part of the recorded image. By selecting individual video line-scans in the optical images, the time resolution was improved to a maximum of 7,550 lines/s (132 μs/line). As a result, detailed time courses of the calcium responses were recorded using high-speed scanning with our micro-endoscope (Yashiro et al., 2017b).

1.10   Organization

This dissertation is organized as follows. Chapter 2 describes the micro-endoscopic system. Chapter 3 contains the details of the simultaneous optical and electrical recordings that were performed in mouse IC. Chapter 4 presents the results of the first investigation of calcium imaging in the IC of the bat. Chapter 5 discusses the improvements that were made in the time resolution of the optical imaging and the detailed time course of the calcium responses that were evoked by sound stimuli. Chapter 6 describes the optical responses and electrical activities that were evoked by mimic pulse and echo sounds. Finally, Chapter 7 draws the conclusions of this dissertation and describes the possible directions for future research.

CHAPTER 2.

Micro-Endoscopic System for Functional Assessments of Neural Circuits in Deep Brain Regions

2.1 Introduction

Simultaneous recording of neural activity from many individual neurons is essential to understand how neuronal circuits work. Multiple electrodes, such as tetrodes, are often used for that purpose. The electrophysiological recording has fine temporal resolution (< 0.1 ms), however, the spatial information obtained is limited, because of the limited number of electrodes and their spatial configurations. Optical recordings of neural activities have been reported to efficiently overcome this limitation (Rochefort et al., 2008; Grewe and Helmchen, 2009; Grienberger and Konnerth, 2012; Schulz et al., 2012; Ito et al., 2014; Barnstedt et al., 2015). Among which, multi-photon excitation microscopy is especially advantageous because of its high spatial resolution (< 1 μm) and the ability to observe deeper tissue than epi-fluorescence microscopy (Helmchen and Denk, 2005; Sullivan et al., 2005; Mank et al., 2008; Rochefort et al., 2008; Murayama and Larkum, 2009; Bandyopadhyay et al., 2010; Bathellier et al., 2012; Grienberger et al., 2012; Grienberger and Konnerth, 2012; Schulz et al., 2012; Horton et al., 2013; Issa et al., 2014; Barnstedt et al., 2015). However, the deepest observable depth is still around 800 μm from the brain surface (Helmchen and Denk, 2005), and in vivo recording from further deep areas remains difficult.

Several studies suggest that insertion of optical fiber bundles into deep areas may be effective in overcoming this limitation (Flusberg et al., 2005; Vincent et al., 2006; Murayama et al., 2007; Rochefort et al., 2008; Grewe and Helmchen, 2009; Murayama and Larkum, 2009; Grienberger et al., 2012; Grienberger and Konnerth, 2012; Hayashi et al., 2012; Schulz et al., 2012; Osanai et al., 2013).

In this chapter, we present data from our newly designed micro-endoscopic system that enables optical recordings of neuronal responses through the optical fiber bundle from deep brain regions. The results demonstrate the potential of our technique in mapping neuronal circuits in deep brain areas.

2.2 Materials and Methods

2.2.1 *Animals*

Optical recording experiments were conducted on mutant mice in which the cellular nucleus of all the cells were ubiquitously labeled with YFP (Kamioka et al., 2012) or CBA mice. Under anesthesia (90 mg/kg ketamine, 5 mg/kg xylazine), fur and skin were removed from the head and a craniotomy was performed over the IC. An aluminum head plate was attached to the skull to fix the head during experiments. In case of CBA mice, calcium sensitive Oregon green 488 BAPTA-1, AM (OGB, invitrogen, Waltham, MA, USA) was injected to label the cells. All protocols were approved by the Animal Research Committee of the Osaka Bioscience Institute.

2.2.2 *Loading of Ca^{2+} sensitive fluorescence indicator dyes*

OGB solution (0.8 mM, in a solution of 160 mM NaCl, 5 mM KCl, 1 mM MgCl2, 2.5 mM CaCl2, 10 mM glucose, 5 mM HEPES-NaOH) was loaded into glass micropipettes (GD-1.2, Narishige, Tokyo, Japan, tip diameter: 5-8 mm) fabricated using a puller (P-87, Sutter Instruments, Novato, CA, USA). OGB solution (1.0 μL) was injected by pressure into the IC at depths of 250, 650, and 1,050 μm from the brain surface.
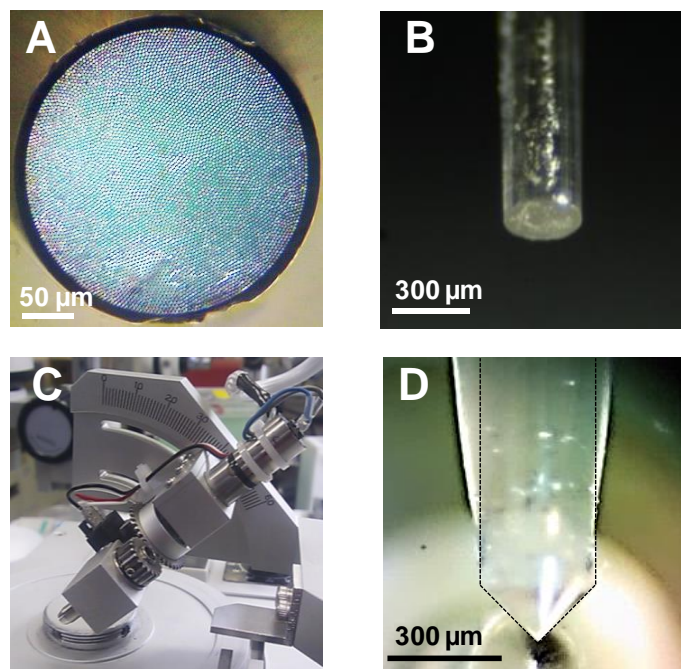
Figure 2.1 Optical fiber bundle to use as an endoscope tip
(A) A photograph of one end of the fiber bundle polished to create an optically flat surface. **(B)** A photograph of the tip of the endoscope before being beveled. **(C)** A photograph of the optic fiber beveller. **(D)** The tip of the endoscope to be inserted into the brain. The tip was beveled to be cone-shaped for minimally disruptive insertion.

2.2.3 *Fabrication of the micro-endoscope probe*

The micro-endoscope was fabricated from a commercially available fiber bundle of 3,000 or 6,000 single-mode fibers (FIGH-215S or 300S, Fujikura Ltd., Tokyo, Japan, Figs. 2.1A and B). We beveled the tip of the fiber bundle to be cone-shaped (slope angle was set to 45°, Fig. 2.1D) using an optic fiber beveller (Oshima Shisaku, Tokyo, Japan, Fig. 2.1C) to minimize invasion upon inserting the probe into brain. The other end of the fiber bundle was polished to obtain an optical flat surface (Fig. 2.1B), and scanned with a resonance galvano-mirror (CRS 4 kHz, GSI Lumonics Inc., Billerica, MA, USA, Figs. 2.2B and C) based laser scanner through an objective lens (MPlan 20x, numerical aperture (NA) = 0.4, Olympus, Tokyo, Japan). The field of view was 215 or 300 μm in diameter, corresponding to the diameter of the fiber bundle. The distance between each optic fiber core, which determines spatial resolution, was around 3.5 μm. The diameter of each optic fiber was around 2 μm. The light spread angle from the endoscope, as calculated from NA of the fiber bundle (ca. 0.4) and the refractive index of the brain tissue (ca. 1.3), was about 36°.

2.2.4 *Hardware and software for acquiring endoscopic image*

We used a solid-state blue laser (488 nm, 60 mW, Melles Griot, Carlsbad, CA, USA) for excitation light source. Fluorescence signal was detected by a photo multiplier (R3896, Hamamatsu, Shizuoka, Japan) through an emission filter (FF01-520/35-25, Semrock, Rochester, NY, USA) and stored on a PC through a non-standard analogue frame grabber (PCI-1409, National Instruments, Austin, TX, USA) (Fig. 2.2A). The pixel clock frequency was set to 10 MHz, and the resolution of raw image was set to

1,250 (Horizontal) × 400 (Vertical) pixels (Fig. 2.3A). The time required to obtain one whole frame was 50 ms. We set the interval between frames (time interval between the bottom line of the previous frame and the top line of the current frame, which is required to wait for the Y axis galvano motor (G120, GSI Lumonics Inc., Billerica, MA, USA, Figs. 2.2B and C) to return from bottom to top) as 3 ms. Thus, the endoscopic image was acquired at every 53 ms. We used MATLAB and Image Acquisition Toolbox to control the frame grabber.
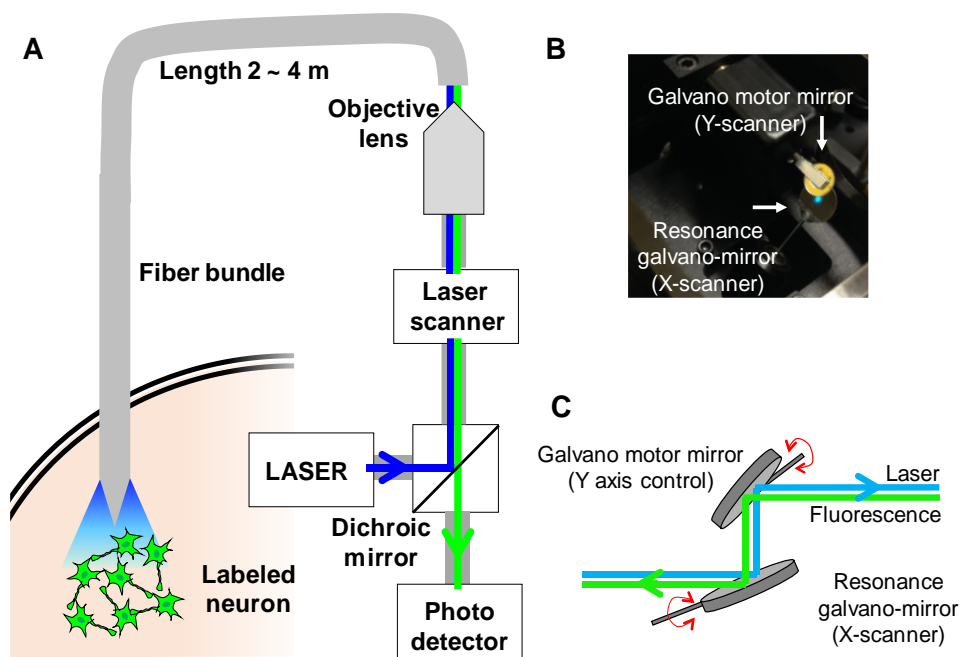
Figure 2.2 Micro-endoscope system for optical recording
(A) Schematic drawing of the micro-endoscope system. **(B)** A photograph of laser scanning mirrors. **(C)** Schematic drawing of the scanning mirrors.
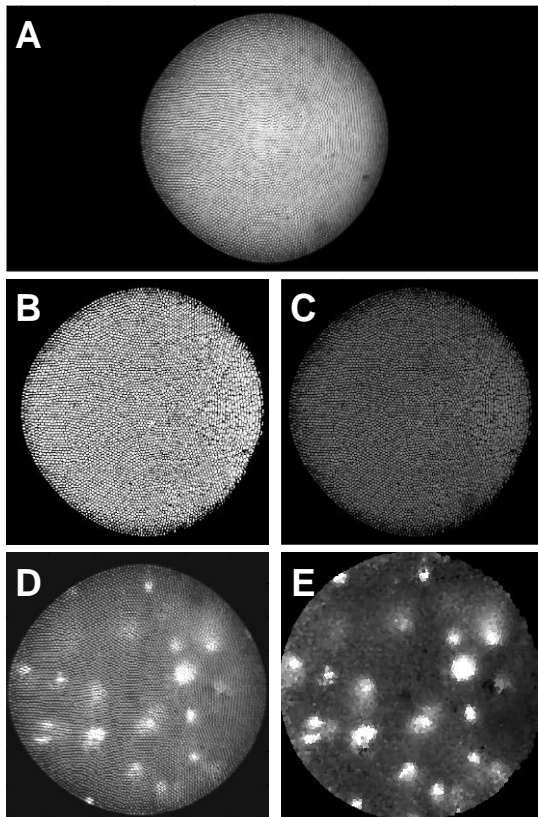
Figure 2.3 Processing of the micro-endoscopic images
(A) A micro-endoscopic image that was averaged 100 times. The probe tip was dipped in a green fluorescent solution (10 µM of Uranine). **(B)** A micro-endoscopic image that was averaged to obtain the value of a white pixel. **(C)** A micro-endoscopic image that was averaged to obtain the value of a black pixel. The probe was dipped in purified water. **(D)** An example of a raw micro-endoscopic image that was recorded when the tip was dipped in a liquid containing fluorescent microbeads. **(E)** An example of a compensated micro-endoscopic image, which resulted from processing the image in Fig. 2.3D.

2.2.5 *Image processing*

In in vivo imaging using fiber bundles, each fiber's core acts as a 'pixel', *i.e.*, each fiber bundle provided 3,000 to 6,000 fluorescence data points corresponding to the number of fibers. Several papers have described the software compensation of images obtained by fiber bundles (Göbel et al., 2004; Perchant et al., 2004; Doroshkevich et al., 2005; Vincent et al., 2006). We similarly processed our data using MATLAB scripts and several C functions as described below. First, we dipped the probe tip into a green fluorescent solution (10 µM of Uranine, similar fluorescence consists of intensity to OGB labeled cells in vivo) and took 100 frames to make one average draw image (Fig. 2.4A). In the averaged image, we determined the location of each fiber

core by finding regional peaks with arbitral size limitations, and linked the pixels of the raw image to each fiber (one fiber core usually consists of around twenty raw image pixels). Next, we averaged the pixel values belonging to each fiber and defined it as 'white' for the corresponding fiber (Fig. 2.3B). Then, we dipped the probe into purified water and similarly averaged pixel values and defined it as 'black' (Fig. 2.3C). So, each fiber has an identification number, raw image pixels belonging to, and black & white values. We compensated the raw image data by linearly interpolating the fluorescence intensities using black & white values and mapping the calculated fluorescence values on the target mosaic picture which were composed of thousands of tiles, the number of which corresponded to that of fibers (Perchant et al., 2004). The shape of the target mosaic picture was set to a circle, indicating that the distortion created by the resonant galvano motor scanning (Leybaert et al., 2005) is compensated through this image processing (Figs. 2.3D and E). Endoscopic image was further smoothed using a gaussian filter in MATLAB or ImageJ (U. S. National Institutes of Health, Bethesda, MD, USA). Upon the analysis of spatial distortion in the micro-endoscopic observation with cone-shaped tip, we adopted polar coordinates to the processed image described above.

2.3 Results

2.3.1 *In vivo micro-endoscopic imaging*

 IC cells labeled with OGB were examined *in vivo* by micro-endoscopy (Fig. 2.4B). To compare its spatial resolution to that of epi-fluorescence microscopy, acute IC slices (thickness: 300 μm) were prepared after *in vivo* micro-endoscopic observation. As shown in Fig. 2.4B, spatial resolution of the image obtained by micro-endoscope appeared not so good as that obtained by epi-fluorescence microscope (Fig. 2.4A). However, it was sufficient enough to discriminate the somata from surrounding tissues.
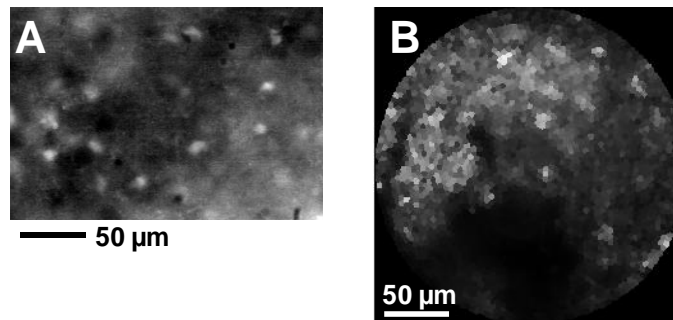
Figure 2.4 *In vitro* and *In vivo* micro-endoscopic images
(A) *In vitro* epi-fluorescence microscopic image of mouse IC labeled with Oregon Green BAPTA-1, AM. **(B)** Micro-endoscopic image of IC similarly labeled to Fig. 2.3A.

2.3.2 *Spatial distortion of endoscopic image using cone-shaped tip*

To minimize the brain damage accompanied by the insertion of probe, we selected cone-shaped tip. However, there was a considerable distortion in the spatial domain because of the tip shape. For clear representation of this spatial distortion, we used a mutant mouse in which the cellular nuclei of all the cells were ubiquitously labeled with YFP (Kamioka et al., 2012) and observed IC circuits by our micro-endoscope. As the probe advanced toward deeper area, the cells located at around the center of the viewfield moved radially to the viewfield edge (Figs. 2.5A and B). When the cell distribution in one endoscopic viewfield was represented in the polar coordinate (Fig. 2.1B), nuclear size of cells observed in the center of the viewfield initially increased with the probe advancement (*e.g.* 'a' in Fig. 2.5A), however it stayed relatively constant in other cells (Fig. 2.5B). The distances between cells located in the closer polar angle did not change much with probe advancement, however, the distances between cells located with larger polar angle differences considerably elongated (Figs. 2.5B and C). Thus, the distance between the cells needs careful interpretation of the results, although the size could be estimated except when the objects were located at around the center of the view-field. Above results also indicate that when the cellular nuclei were labeled as exampled in Fig. 2.5, our endoscope system had enough optical resolution in clearly discriminating cell bodies of individual cells.
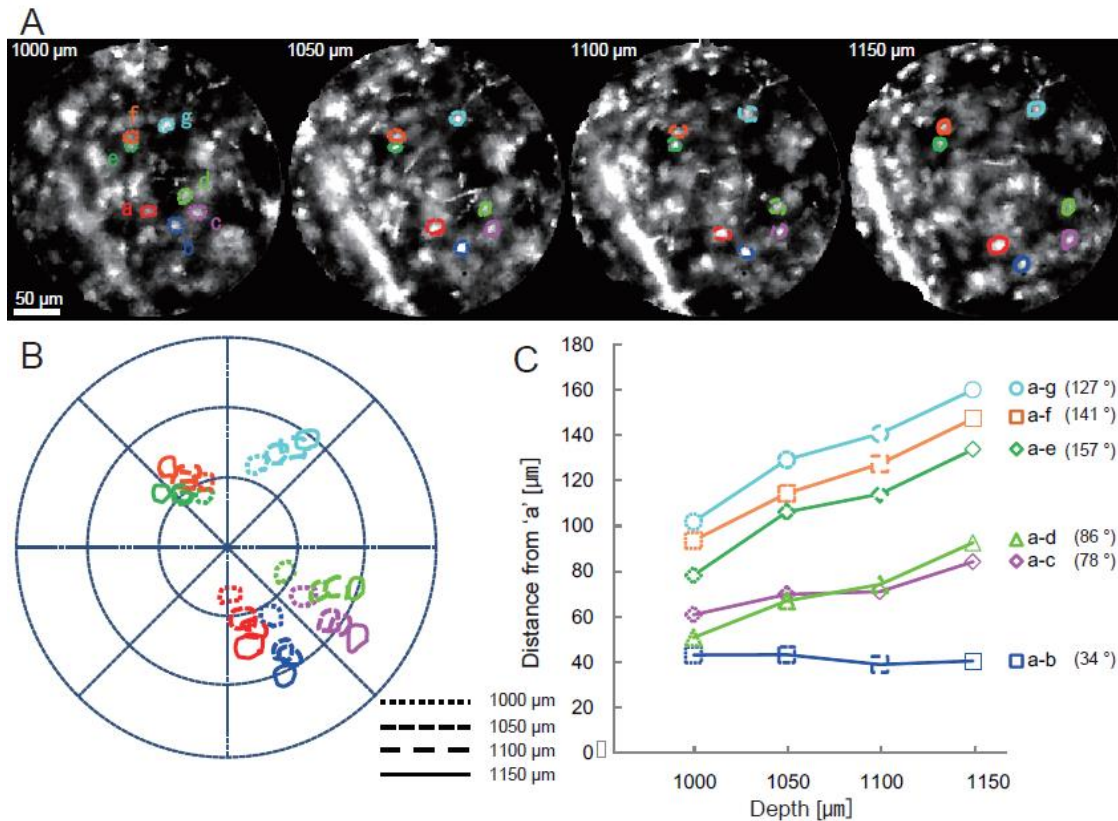
Figure 2.5 Possible spatial distortion with cone-shaped probe tip
(A) Four sequentially recorded micro-endoscopic images upon probe advancement. Bright spots correspond to the nuclei of cells. Seven nuclei were marked with seven different colors and labeled. Numbers at the left top of each image corresponded to the depth of probe tip from brain surface. **(B)** Positional drift and change in size upon probe advancement. In this and other figures, line style indicates the depth of probe as shown in the panel. **(C)** Changes in distance between nuclei upon probe advancement. Distance between nucleus 'a' and other nuclei were plotted against the probe depth. Numbers in parentheses aside symbols in the panel indicate the polar angle differences between nucleus 'a' and other nuclei at a depth of 1,000 μm.

2.4 Discussion

We formed the endoscopic tip to be cone-shaped. We also tried flat surfaces with or without 45 deg slope. The latter (flat surface without slope) would be better in terms of spatial distortion, however it was very hard to be inserted into brain tissue. The former (flat surface with 45 deg slope) was easily inserted, however we sometimes encountered hemorrhage presumably due to the damage of small vessels during insertion. With cone-shaped tip, on the contrary, we have not experienced hemorrhage. Therefore, we adopted this type of tip shape in the present study. Images recorded through our micro-endoscope have sufficient spatial resolution to resolve each cell (Fig. 2.5B). Although the resolution is lower than that of epi-fluorescence (Fig. 2.5A) or single-or multi-photon confocal microscopy, we can detect labeled cell clusters, observed as white grains. Because the size of collicular neurons in mice ranges from 5 to 30 μm (Meininger et al., 1986), and the focal depth of our endoscope probe was approximately around 30 μm (Vincent et al., 2006), recorded cell bodies were likely located within only a single-neuronal layer in the vicinity of the micro-endoscope tip. The spatial resolution of our optical probe was 3.5 μm, which would be enough for most neurons of normal sized cell bodies (>8 μm), however, higher spatial resolution would be appreciated when targeting very small cells, *e.g.*, cerebellar granule cells.

2.5 Summary

The micro-endoscope was developed to perform optical imaging in deep brain regions by combining a laser scanning microscope with an optical fiber bundle that was used as an endoscope tip. By inserting the fiber bundle tip into the brain, the micro-endoscope enabled us to perform optical measurements in deeper areas (over 1,000 μm) in which recordings were difficult to do with a conventional fluorescence microscope. In addition, although the spatial resolution was lower than that of an epifluorescence microscope, the results showed that the spatial resolution was sufficient for the identification of individual cell bodies on the micro-endoscopic images.

CHAPTER 3.

Optical and Electrical Micro-Endoscope Recordings of Auditory Responses in Mouse Inferior Colliculus

3.1 Introduction

 Multiple electrodes, such as tetrodes, are often used for that purpose. The electrophysiological recording has fine temporal resolution (< 0.1 ms), however, the spatial information obtained is limited, because of the limited number of electrodes and their spatial configurations. Our system allows us to compare optically recorded data with those obtained by well-established electrophysiological methods (*i.e.*, local field potentials: LFP, and multi-unit activities: MUA). We selected the inferior colliculus (IC), a key auditory station in midbrain, as a target for measurements because of the availability of detailed anatomical and physiological information (Ehret and Moffat, 1985; Stiebler and Ehret, 1985; Meininger et al., 1986; Rees and Palmer, 1988; Rees et al., 1997; Schreiner and Langner, 1997; Phillips et al., 2001; Portfors et al., 2011) and its inaccessibility with traditional optical recording techniques. The results demonstrate the potential of our technique in mapping neuronal circuits in deep brain areas at fine spatio-temporal resolution. In this chapter, we present data from our newly designed micro-endoscopic system that enables simultaneous optical and electrical recordings of neuronal responses through the same optical fiber bundle, whose tip surrounds were metal coated to work as an electrode.

3.2 Materials and Methods

3.1.1 *Animals*

Optical recording experiments were conducted on CBA mice purchased from SLC Japan (10–24 g, aged 4–12 weeks). Under anesthesia (90 mg/kg ketamine, 5 mg/kg xylazine), fur and skin were removed from the head and a craniotomy was performed over the IC. An aluminum head plate was attached to the skull to fix the head during experiments. We usually added ketamine and xylazine when necessary, *e.g.*, 60–90 min after the initial injection. All protocols were approved by the Animal Research Committee of the Osaka Bioscience Institute.

3.1.2 *Fabrication of the micro-endoscope probe*

The micro-endoscope was fabricated from a commercially available fiber bundle of 3,000 or 6,000 single-mode fibers (FIGH-215S or 300S, Fujikura Ltd., Tokyo, Japan). First, the plastic jacket covering the fiber bundle was chemically denuded using chloroform (Nakalai, Kyoto, Japan) up to 10 mm from the probe tip. Next, the tip was gold-coated using a sputter coater (IB-3, Eiko, Ibaraki, Japan), and then coated with enamel paint (TPU F2-26NC, Tohtoku, Tokyo, Japan) for insulation (Figs. 3.3B and C). By beveling the tip after the above two coatings using an optic fiber beveller (Oshima Shisaku, Tokyo, Japan), only the surrounding edge of the tip became electro-conductive, enabling us to use the endoscope as an electrode for recording or stimulating the circuits under optical observation. The impedance of the electrodes fabricated in this manner was usually around 200 kΩ. Since a resonant galvano motor

generates a tone (4 kHz in this case) that may disturb auditory experiments, confocal optics were placed far from the animal and outside of the sound-proof chamber and connected to the probe via a long fiber bundle (> 2 m). Trans-mission loss of lights by the long fiber bundle was minimal (ca. 2.5 % per meter).
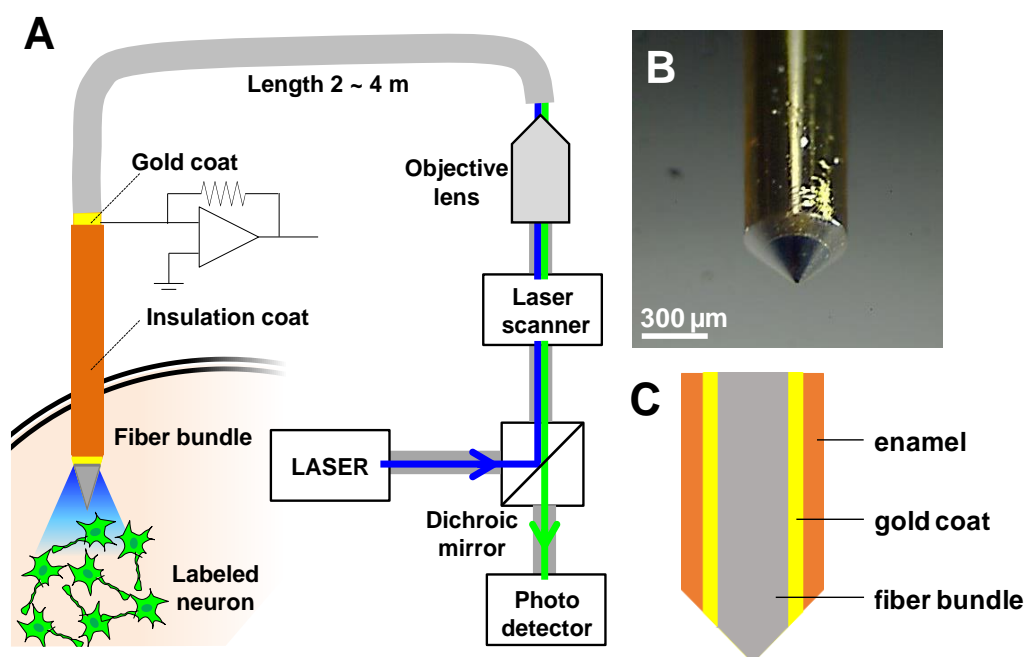
Figure 3.1 Micro-endoscope system for optical and electrical recording
(A) Schematic drawing of the micro-endoscope system. **(B)** The tip of the endoscope to be inserted into the brain. The tip was beveled to be cone-shaped for minimally disruptive insertion and coated with gold and enamel for electrical conduction and insulation, respectively. **(C)** Schematic drawing of the endoscopic tip coated with gold and enamel.

3.1.3 *Acoustic stimuli*

Acoustic stimuli were presented through a ribbon tweeter (TW-III, Pioneer, Kanagawa, Japan) placed in front of the animal in a sound-attenuated chamber (D-50, Sound Japan, Saitama, Japan). The distance between the tweeter and the animal was set to 25 cm. Sound intensity was calibrated using a calibrated condenser micro-phone (4136, Brüel and Kjær, Nærum, Denmark). Stimulus sound wave forms were white noise bursts (2–60 kHz) or tone bursts (5, 7, 10, 15, 20, 30, 40 and 60 kHz), which were computed online using MATLAB (MathWorks, Natick, MA, USA). Sound duration was 50 ms including 5 ms rise and fall with raised cosine function. Sound pressure level was varied from 15 to 95 dB SPL (re: 20 μPa) in 10 dB steps. Inter stimulus interval was about 1 s. Stimulus sound was created by playing the waveform through a 16 bit D/A converter (NI PCI-6259, National Instruments, Austin, TX, USA) at a sampling rate of 200 kHz.

3.1.4 *Loading of Ca^{2+} sensitive fluorescence indicator dyes*

Calcium sensitive Oregon green 488 BAPTA-1, AM (OGB, invitrogen, Waltham, MA, USA), (0.8 mM, in a solution of 160 mM NaCl, 5 mM KCl, 1 mM MgCl2, 2.5 mM CaCl2, 10 mM glucose, 5 mM HEPES-NaOH) was loaded into glass micro-pipettes (GD-1.2, Narishige, Tokyo, Japan, tip diameter: 5–8 mm) fabricated using a puller (P-87, Sutter Instruments, Novato, CA, USA). OGB solution (1.0 μL) was injected by pressure into the IC at depths of 250, 650, and 1,050 μm from the brain surface.

3.1.5 *Optical recording by micro-endoscope*

Thirty minutes after dye loading, the micro-endoscope was inserted into the IC (0.5–1.5 mm anterior, 0.0–2.0 mm lateral from lambda, 0.0–1.5 mm depth from the brain surface) by a motorized micro-manipulator (MM-3, Narishige, Tokyo, Japan, modified to work with CMA-25CCCL, ESP300, Newport, Irvine, CA, USA). Suitable recording locations were identified by both optical and electrical responses to sound stimuli (50 ms of white noise burst,85 dB SPL) periodically presented at approximately 1 Hz. Usually finding good recording locations by optical response was more difficult than that by electrical recordings.

3.1.6 *Electrophysiological recording*

Electrical signals recorded from the edges of the micro-endoscope tip were impedance-converted using a bridge amplifier (Axoclamp2A, Molecular Devices, Sunnyvale, CA, USA), band-pass filtered (1–10 kHz), amplified (7P511, Grass Technologies, Warwick, RI, USA), hum-noise eliminated (Humbug, Quest Scientific, Vancouver, Canada), and stored on a PC through an A/D converter (PCI-6259, National Instruments, Austin, TX, USA) at a sampling rate of 20 kHz. Electrical signals were separated into LFPs (4–50 Hz) and MUA (300–5000 Hz) using a digital filter in MATLAB. To quantify the amount of MUA evoked by sound, we used root mean square values of the traces during sound stimuli.

3.1.7 *Image processing*

Endoscopic image was smoothed using a gaussian filter in MATLAB. To calculate the change in fluorescence ($\Delta F/F$), the average fluorescence of the four frames before sound presentation (baseline fluorescence: F) was subtracted from the fluorescence obtained in each frame during and after sound presentation.

3.1.8 *Experimental Design*

In optical recording with micro-endoscope, first, the fiber tip was brought into contact with the surface of the IC. Then, pre-stimuli were presented at a period of approximately 1 Hz (every 20 frames) to seek the places where fluorescence change could be observed. To increase the synchronization of the neural activities, 90-dB WN bursts were used as the pre-stimulus because the fluorescence intensity of OGB has been reported to increase proportionally with the number of spikes (Ikegaya et al., 2005). If changes in fluorescence were seen in the averaged data for approximately 30 to 40 s while the pre-stimulus was presented every 20 frames, the measurements were started at that depth. The data recorded during the 30 s can be calculated by averaging the data of each second 27 times. Usually, 558 frames are included in the 30 s of data, and we only used the first 540 frames to calculate the averaged 20 frames (averaged fluorescence: F). Subsequently, the average fluorescence of the first 4 frames in F was subtracted from the fluorescence obtained in each frame to determine the fluorescence change from baseline (ΔF) and the fractional change in fluorescence ($\Delta F/F$). To perform these processes, we wrote MATLAB codes so that we can confirm the auditory responses immediately after recording. The stimulus was presented at the sound pressure level of the sound stimulation from 90 dB and subsequently decreased

in 10 dB steps. If a response was not observed, we used the other sound stimulus and presented at 90 dB again. Because OGB did not work in regions deeper than approximately 1,500 μm, the endoscope tip was withdrawn and inserted into another IC region after recording at the deepest area. Optical measurements were subsequently conducted again in the same way.

Electrophysiological data were recorded simultaneously with optical measurement. While electrophysiological activities were enough signal to noise ratios even without averaging, we calculated these into 27 times averaging of 1 s data because the data lengths were also 30 s. These raw data were separated into LFPs and MUA using MATLAB.

3.3 Results

3.3.1 *Optical and electrical recordings of neuronal activities*

Neuronal responses to a sound stimulus (white noise, 65 dB SPL) presented during the 5th frame (horizontal bar in Fig. 3.2D bottom) were recorded both optically (Figs. 3.2A and B) and electrically (Figs. 3.2C and D) and were shown after averaging of 27 individual trials. The maximal amplitude of the Ca^{2+} (optical) response (Figs. 3.2A and B) appeared 53–106 ms after stimulus onset (6th frame). In most cases, within 53 ms after the sound stimulus onset (5th frame), the optical responses appeared, were limited to the lower region of the viewfield (5th frame in Fig. 3.2A). This pattern was due to the method of endoscopic recording; we scanned the viewfield from top to bottom using a point-scanning laser. Thus, care needs to be taken when interpreting temporal

aspects of optically recorded Ca^{2+} responses. The LFPs and MUA were recorded at the same time as the optical response (Figs. 3.2C and D, respectively). The LFP was characterized by a prominent positive deflection (upward) after the onset of the sound stimulus, followed by a negative deflection (downward, Fig. 3.2C). The multi-unit trace showed sustaining unit activities during the stimulus, which returned to baseline levels immediately after it ended (Fig. 3.2D). Thus, the high temporal resolution of LFPs and MUA could supplement optical recordings.
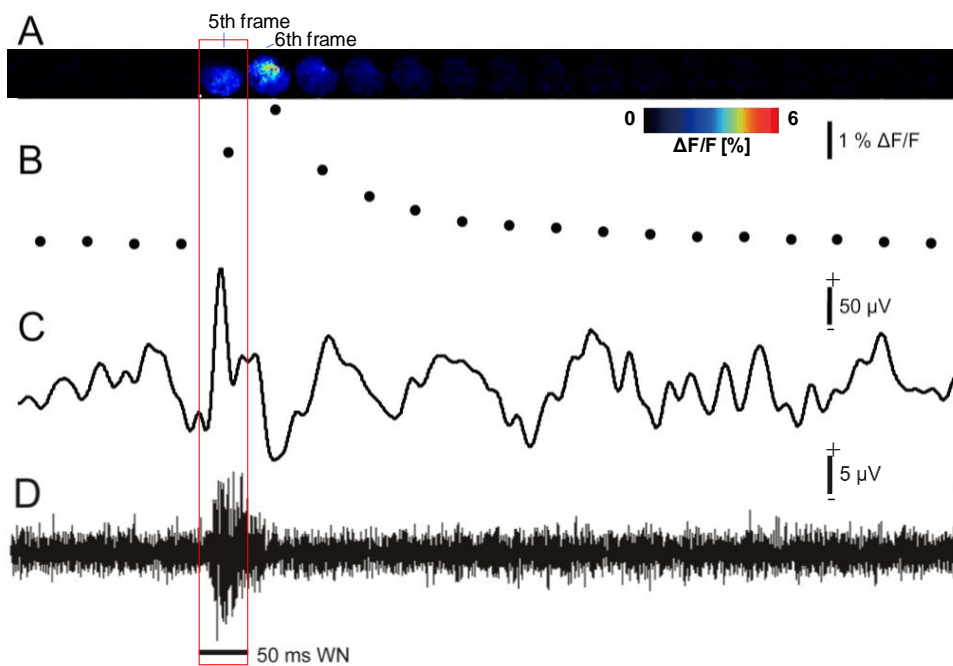
Figure 3.2 Optically and electrically recorded neuronal responses
(A) An example of optically recorded Ca^{2+} response ($\Delta F/F$). A white noise (WN) burst (85 dB SPL, 50 ms in duration) was applied during the 5th frame indicated by a horizontal bar. Field of view, 300 μm. **(B)** Viewfield-wide averaged Ca^{2+} response over time. **(C)** LFP and **(D)** MUA simultaneously recorded with the optical response.

3.3.2 *Intensity-dependent changes*

To examine whether in vivo micro-endoscopic recording could be used to measure response latencies, we systematically changed the sound pressure level from 15 to 95 dB (One example was shown in Fig. 3.3, recorded at depth of 380 μm from brain surface). Significant responses were observed at sound pressure levels above 25 dB both in the optically recorded Ca^{2+} response (green) and in LFP (red) and multi-unit data (blue). Precise analysis of response latency was possible using LFP and MUA data (Fig. 3.3C). Within the first 50 ms after stimulus onset (*i.e.*, the 5th optical image frame), response latencies became shorter with increasing sound pressure level (*e.g.* from 13 ms at 25 dB to 7 ms at 95 dB when measured at the first positive LFP peak). These results further support the usefulness of electrophysiological recording via the endoscopic probe and emphasize its higher temporal resolution. The Ca^{2+} fluorescence, LFPs, and MUA indicated different responses to changes in sound pressure level. The positive deflection in LFPs at sound onset increased steadily with increasing sound pressure level (Fig. 3.4A). MUA increased steeply with sound pressure level up to 35 dB, increased gently above 45 dB, and dropped slightly at the higher sound pressure level tested (above 75 dB) (Fig. 3.4B). The Ca^{2+} responses initially increased with sound pressure level, reaching a maximum at 55 dB, and decreased at higher sound pressure levels (Fig. 3.4C). Thus, the Ca^{2+} response was more similar to MUA than to LFP amplitudes in this example.

31
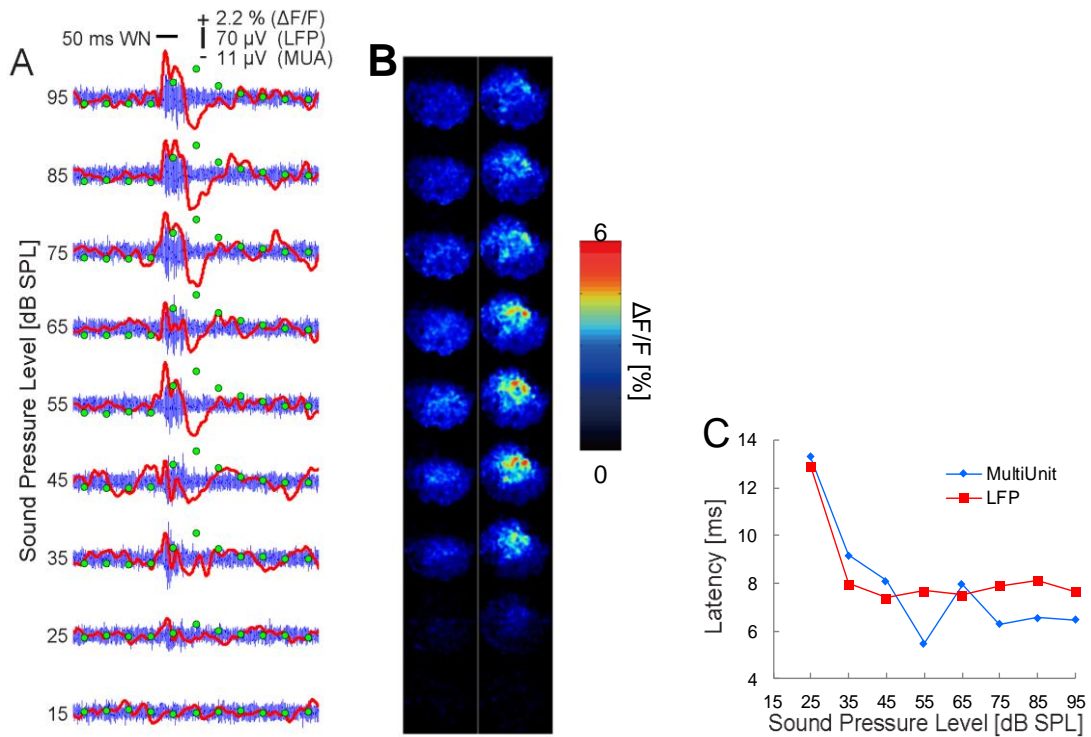
Figure 3.3 Optically and electrically recorded neural responses to sounds of varying intensity

(A) Optical and electrical responses to various sound pressure levels (15 - 95 dB SPL). Green dots, viewfield-wide averaged optical responses; red lines, LFPs; blue lines, MUA. **(B)** Micro-endoscopic images of the stimulus frame (left column, 0 - 53 ms, 5th frame) and the peak frame (right column, 53 - 106 ms, 6th frame) of Ca^{2+} (optical) response ($\Delta F/F$) to several sound intensities. Field of view = 300 µm. Sound (white noise) was applied during 5th frame. **(C)** Latency-level functions of LFP and MUA. Latency was measured at the first positive peak in LFP or the time when it exceeded the point of 2.5 times standard deviation of the background noise (before sound) in MUA.
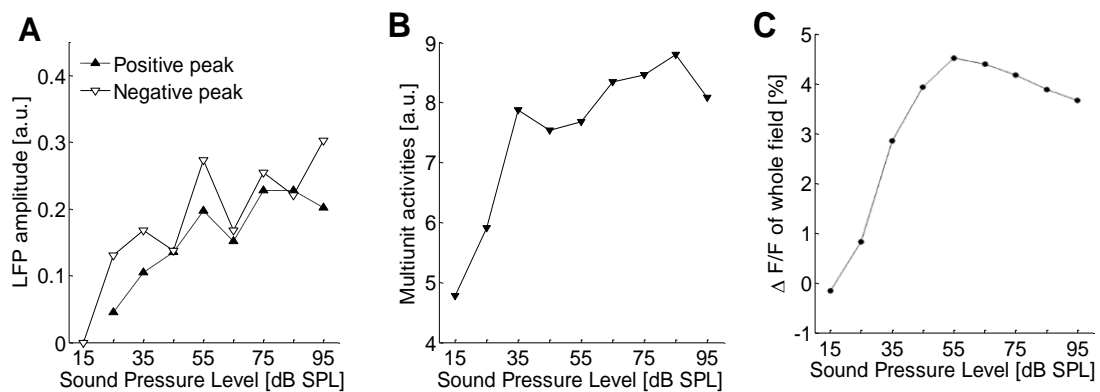
Figure 3.4 Dependence of sound pressure level for LFPs, MUA and Ca²⁺ response

(A) Relationships between sound pressure level and LFPs (red in Fig. 3.4A). Peak amplitudes of positive (filled triangle) and negative (open triangle) deflections versus sound pressure level. **(B)** Sound level dependence of MUA (blue in Fig. 4A). **(C)** Sound level dependence of averaged Ca²⁺ responses across the viewfield.

3.3.3 *Spatial difference in single viewfield*

In some of data, we found spots whose area size corresponded to that of IC neurons (10–30 μm in diameter, Fig. 3.5A). By separately analyzing individual spots, we could observe independent response properties to changes in sound pressure level for each spot. Although, additional labeling of cell bodies with different fluorescent color is appreciated to identify the location of individual cell bodies in OGB labeling, our system is supposed to have enough spatial resolution to analyze individual cell-response variability. Above results also indicate that our system would be useful in other neurophysiological studies comparing electrically recorded phenomena with optically recoded responses.
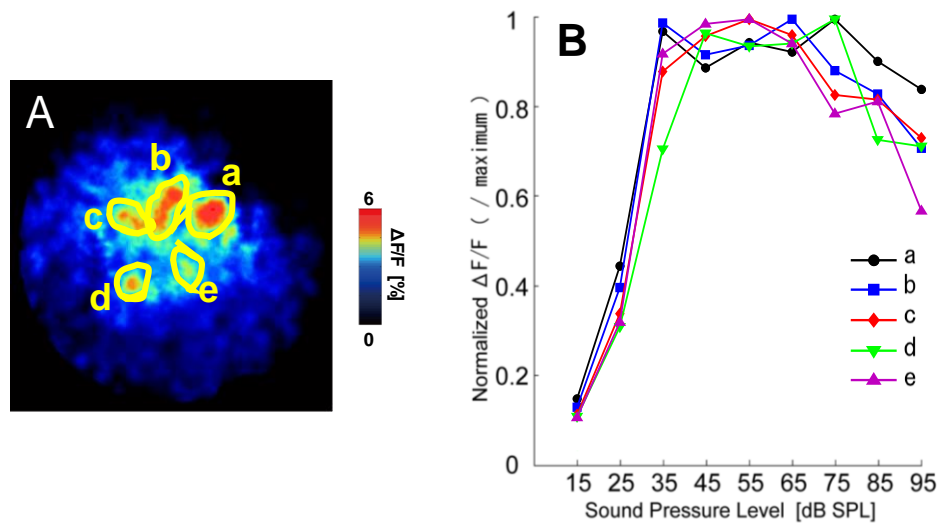
Figure 3.5 Spatial difference of calcium responses in single viewfield
(A) Five hot spots (a - e) observed in one endoscopic viewfield are circled. Field of view = 300 μm. **(B)** Sound level dependence of Ca^{2+} responses corresponding to five areas labeled in Fig. 3.7A. All curves were normalized against peak responses.

3.3.4 *Frequency-dependent changes in optical responses*

To assess whether our system could detect dorso-ventral topographic organization in the IC, we systematically changed the depth of the micro-endoscope probe (depths of 150, 500, and 1,500 μm) while recording Ca^{2+} responses to tone bursts at varying sound frequencies (5, 7, 10, 15, 20, 30, 40, and 60 kHz) and sound pressure levels (25–95 dB SPL at 10 dB steps) (Fig. 3.6). Some Ca^{2+} responses were observed even at 25 dB SPL with 7 kHz tone bursts at 150 μm depth (Fig. 3.6A), whereas at 500 μm depth, the most sensitive and robust responses were observed at 15 kHz (Fig. 3.6B). Similarly, when the probe was placed 1,500 μm below the brain surface, the frequency that elicited the greatest response shifted even higher to 30 kHz (Fig. 3.7). These results are in agreement with previous reports of the tonotopic organization of the IC with unit recordings; dorsally located cells respond more intensely to lower frequencies and

ventrally located ones more to higher frequencies, respectively (Schreiner and Langner, 1997; Portfors et al., 2011), confirming the usefulness of our recording system for examining the spatial organization of deep brain regions.
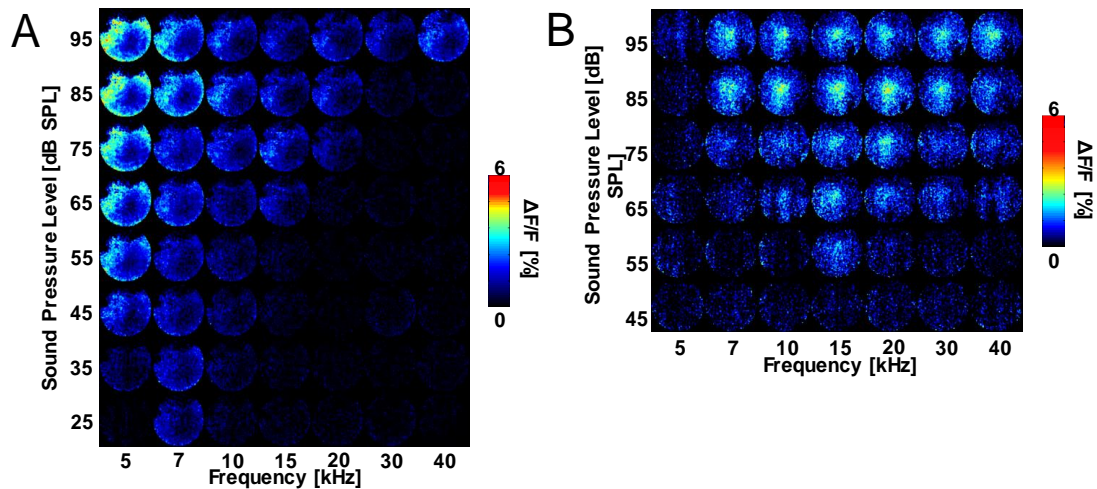
Figure 3.6 Frequency-dependent change in Ca^{2+} responses
(A) Ca^{2+} response profile at 150 µm from the brain surface. X-axis, frequency; y-axis, sound pressure level of stimulus (tone burst). Each image represents the frame with maximum response. **(B)** Ca^{2+} response profile at 500 µm from the brain surface.
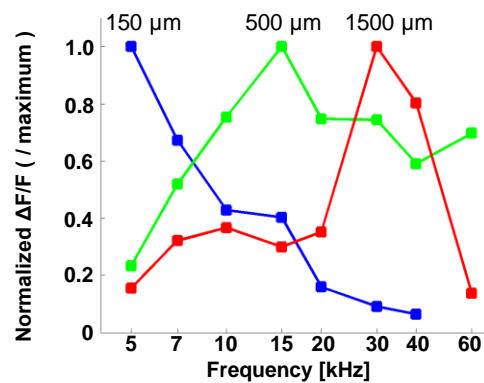
Figure 3.7 Ca^{2+} responses recorded at three different depths (150, 500, and 1500 µm) in IC
Frequency dependent changes in optical responses recorded at three depths from the brain surface with a fixed sound intensity (65 dB SPL).

3.4 Discussion

3.4.1 *Auditory responses*

We observed Ca^{2+} responses ($\Delta F/F$) to sound stimuli in the range of 3–6 % (Figs. 3.2–3.5), comparable to previous reports (Grienberger and Konnerth, 2012; Schulz et al., 2012). For example, fluorescence changes in the somato-sensory cortex recorded through optical fibers upon electrical stimulation of fore- and hindpaws were less than 10 %(Schulz et al., 2012). However, the same study also reported that signal changes using a two-photon excitation microscope ranged from 40 to 100 % (Schulz et al., 2012). This difference in the signal change likely results from a general difference between imaging methods; another two-photon microscopy study using OGB observed signal changes of 25–60 % in the auditory cortex (Grienberger and Konnerth, 2012). Importantly, response latencies of LFPs and MUA were elongated with decreasing sound pressure level (Fig. 3.5C). This intensity-latency relationship has been reported in several neurophysiological studies of IC circuits using electrodes (Pedemonte et al., 1997; Klug et al., 2000). These results, thus, indicate that our system accurately recorded electrophysiological responses in addition to optically measured responses.

3.4.2 *Simultaneous optical and electrical recordings*

Our endoscope system recorded auditory responses both optically and electrically. While the temporal resolution of Ca^{2+} responses was limited (Fig. 3.2B), the optical recordings allowed resolution of individual cells (Fig. 2.5). Electrophysiological

recordings, on the other hand, proved to serve a complementary role. While they did not provide any spatial information (because we used only one electrode), they did provide greater temporal resolution than optical recordings. Simultaneous optical and electrical recordings can thus supplement each other by providing fine spatial and temporal information, respectively. Our endoscope for simultaneous optical and electrical recording enabled detailed comparison between LFPs, MUA and Ca^{2+} responses (Figs. 3.3–3.4). The fluorescence intensity of OGB was reported to increase proportionally with the number of spikes (Ikegaya et al., 2005), however, it was also reported to reflect subthreshold response (Bandyopadhyay et al., 2010). LFPs were supposed to reflect the sum of synaptic current flowing around the vicinity of electrodes (Kajikawa and Schroeder, 2011; Osanai et al., 2013). Detailed comparison between the optically recorded Ca^{2+} response and several electrophysiologically recorded phenomena, which our system enables, will thus contribute to the better understanding of the physiological role of Ca^{2+} responses.

3.4.3 *Frequency-dependent changes*

Response magnitude changed systematically with changes in sound pressure level and frequency, indicating that we observed the frequency tuning of the recording site (Fig. 3.6A). Optical signal increased with sound pressure level; the frequency that evoked an observable change in the optic signal at the lowest sound pressure level was 7 kHz, which may be analogous to the characteristic frequency observed in unit recordings (Pena et al., 2001). The frequency that elicited the largest response shifted to lower frequencies (5 kHz) as the stimulus intensity increased (Fig. 3.6A). In most

cases, the size of an area activated by sound (Figs. 3.2A, 3.3B, and 3. 5A) was larger than that of IC neuron's cell body (5–30 μm; (Meininger et al., 1986). This difference is in agreement with previous findings that fluorescence changes in OGB result from Ca^{2+} changes at both cell bodies and dendrites (Grienberger and Konnerth, 2012). As seen in Fig. 3.6A, a large portion activated by stimulus appeared to be similarly modulated, with little difference in the location or size of activated areas between different stimuli. The width of a single frequency layer has been reported to be approximately 120–180 μm (Schreiner and Langner, 1997), while the size of our field of view was 300 μm. This system might enable us to observe a few frequency laminae simultaneously, if the penetrate angle is perpendicular to the layers. In addition, a unit recording study determined the characteristic frequency difference between adjacent neurons in the IC to be 0.3 octaves (no more than 2 octaves) (Schreiner and Langner, 1997; Chen et al., 2012), while the frequency resolution in our protocol was approximately 0.5 octaves. Therefore, our field of view may have contained more than two frequency areas.

3.4.4 *The difficulty and reproductively of this method*

Capturing auditory response electrically has become very stable recently, without failure (*e.g.* 5 out of 5 animals), although we initially encountered several troubles with electrical recordings, mainly due to the unstable electrical contact between the probe and the preamplifier. Optical recording was more difficult than electrical recording presumably because the tissue with optimized concentration of Ca^{2+} dye was restricted to a relatively small area and was not easily hit by the probe. To increase the success

ratio, we modified the electrode holder so that it can hold either the glass capillary for dye loading or the micro-endoscope for response recording. With such modification, our recent success rate in capturing auditory response optically was 75 %, *e.g.*, 3 out of 4 animals. As to the reliability or reproducibility of recording, it strongly depended on the time required to collect data. It usually took c.a. 30 s (*i.e.* 27 times averaging of 1 s data) to obtain clear optical and electrical responses to one sound condition, as was exemplified in Fig. 3.2 (with almost no spontaneous baseline activity in the optical data). Also, we wrote MATLAB codes to analyze optical data after one series of dataset was achieved, to know the recording condition online. This analysis took more than 1 min for each dataset. Thus, it took more than 90 s to obtain a dataset for one sound condition. In the series of experiments such as in Fig. 3.6, in which response has to be recorded with several sound conditions (56 conditions in Fig. 3.6A), the time required to collect all the data was consider-ably long (*e.g.* more than 90 min in Fig. 3.6A). It was difficult to keep stable anesthetic state throughout such a long-time measurement. Therefore, we do not have other optical datasets of frequency tuning curve than were presented in Fig. 3.6. However, experiments with a single (Fig. 3.2) or a small number of sound conditions (Fig. 3.3: 9 conditions), we have many other datasets (*e.g.* 19 optically recorded datasets for level-rate function, as Fig. 3.3). Most data (Twelve out of nineteen) showed non-linear rate-level function as was exemplified in Fig. 3.4.

3.5 Summary

Simultaneous optical and electrical recordings were conducted with the micro-endoscopic system. The fiber tip was coated with gold and enamel, so it could be used as an electrode for the electrophysiological recordings. Thus, the optical responses and electrical activities were recorded from the same area. The simultaneous recordings of the stimulus intensity-dependent profiles of the Ca^{2+} responses and the local field potentials (LFPs) and multiunit activities (MUA) allowed for examinations of the relationships among these responses. In addition, we found spots whose sizes corresponded to those of the IC neurons. By separately analyzing the individual spots, we observed independent response properties to changes in SPLs for each spot. Thus, the temporal resolution of the Ca^{2+} responses was limited, whereas the optical recordings allowed a resolution that was sufficient for examining individual cells. However, the electrophysiological recordings provided temporal information. Therefore, simultaneous optical and electrical recordings can supplement each other by providing data with fine spatial and temporal resolution, respectively.

CHAPTER 4.

Optical Micro-Endoscope Imaging of the Bat Inferior Colliculus

4.1 Introduction

In this chapter, we will describe the calcium imaging that was performed in the bat IC to establish a method for performing optical measurements. To our knowledge, calcium imaging using bats as subjects has never been conducted, and the methods have not been established. Therefore, we applied the experimental procedures that were established with mice, as described in Chapter 3. Optical measurements were performed using the micro-endoscope on short-tailed fruit bats (*C. perspicillata*). The changes in fluorescence related to the auditory responses to the white noise (WN) bursts and FM sweep sounds were recorded.

4.2 Materials and Methods

4.2.1 *Animals*

The subjects were 2 short-tailed fruit bats (C. perspicillata). Mixed anesthetic (Medetomidine: 0.4 mg/kg, Midazolam: 4.0 mg/kg, Fentanyl: 0.4 mg/kg) was injected into the bat intraperitoneally. The anesthetized bat was then placed on an aluminum

41

platform, wrapped in cotton gauze with a hand warmer (Iris Oyama Co, Sendai, Japan) placed on its back to maintain body temperature in the range of 25–30 ºC. After removing fur and skin of their head, the medial tendon (origin point) of temporal muscle was cut and pushed to lateral direction to expose the skull. Then, a craniotomy was performed over the inferior colliculus (IC). Since their IC was covered with transverse sinus (TS) and the cerebellum (Cb), we pushed away TS and Cb to caudal and rostral directions respectively to expose the IC. All protocols were approved by the Animal Research Committee of Brown University.

4.2.2 *Acoustic stimuli*

Sound stimuli were downward frequency modulated sounds (FM: 100 to 30 kHz), and white noise bursts (WN: 5-100 kHz). The sound duration was 50 ms including 1 ms rise and fall times with raised cosine slope. Sound pressure level was varied from 10 to 90 dB SPL (re: 20 µPa) in 10 dB steps. Stimulus sound was created by playing the waveform, which was computed online using MATLAB (MathWorks, Natick, MA, USA), through a 16 bit D/A converter (NI PCI-6259, National Instruments, Austin, TX, USA) at a sampling rate of 200 kHz. These acoustic stimuli were presented from a loud speaker in a sound-attenuated chamber. The distance between the speaker and the animal was set at 25 cm. The sound stimuli were periodically presented at approximately 1 Hz (every 20 frames) while recording.

4.2.3 *Loading of Ca^{2+} sensitive fluorescence indicator dyes*

Oregon green 488 BAPTA-1, AM (OGB, Thermo Fisher Scientific, Waltham, MA, USA) was diluted with saline to be 0.8 mM and loaded into a glass micro-pipette, which was fabricated using a puller (PE-2, Narishige, Tokyo, Japan). OGB solution (1.0 µL) was injected by air pressure into the IC at depths of 250, 650, and 1,050 µm from the dorsal brain surface.

4.2.4 *Experimental Design*

Sixty minutes after the dye injections, the fiber tip was positioned on the surface of the IC. The pre-stimuli were presented at a rate of approximately 1 Hz (every 20 frames) to allow observation of the sites of fluorescence changes. To increase the synchronization of the neural activities, 90-dB WN bursts were used as the pre-stimulus because the fluorescence intensity of OGB has been reported to increase proportionally with the number of spikes (Ikegaya et al., 2005). Although the changes in fluorescence were sometimes confirmed without averaging in our previous experiment conducted in mice, the changes could not be seen without averaging in the bats. For this reason, we advanced the endoscope tip by 50-µm steps from the surface of the IC to a depth of approximately 1,500 µm and examined whether the changes in fluorescence could be confirmed at each depth. If changes in fluorescence were seen in the averaged data for approximately 30 to 40 s while the pre-stimulus was presented every 20 frames, the measurements were started at that depth.

In the mouse experiments, 30 s was sufficient to record clear optical and electrical responses to one sound condition (Yashiro et al., 2017a). Hence, the recording time for each condition was set to 30 s in the bats. The data recorded during the 30 s can be calculated by averaging the data of each second 27 times. Usually, 558 frames are included in the 30 s of data, and we only used the first 540 frames to calculate the averaged 20 frames (averaged fluorescence: F). Subsequently, the average fluorescence of the first 4 frames in F was subtracted from the fluorescence obtained in each frame to determine the fluorescence change from baseline (ΔF) and the fractional change in fluorescence ($\Delta F/F$). To perform these processes, we wrote MATLAB codes (The MathWorks, Inc., Natick, MA, USA) so that we could confirm the auditory responses immediately after the recordings. The stimulus was presented at the SPL of the sound stimulation at 90 dB and subsequently decreased in 10-dB steps. If a response was not observed, we used the other sound stimulus and presented at 90 dB again. Because OGB did not work in regions deeper than approximately 1,500 μm, the endoscope tip was withdrawn and inserted into another IC region after recording at the deepest area. Optical measurements were subsequently conducted again in the same way.

4.3 Results

4.3.1 *Optical recordings of neuronal activities*

Endoscopic images of the optical responses (% change in $\Delta F/F$) in *E. fuscus* to the WN and FM sounds are shown in Fig. 4.1. The images are of frames of 4 different

times (0–53 ms, 53–106 ms, 106–159 ms, and 159–212 ms) following the onset of the

WN (top row) and FM (bottom row) sound stimuli. The plot in Fig. 4.1B shows the

mean value of *ΔF/F* for each frame of the WN and FM images. The values of *ΔF/F*

increased to reach a peak during the two frames following the sound onset and

subsequently decreased over 6–7 frames following stimulus offset. The time courses

of the responses to the WN and FM sounds were similar (Fig. 4.1B), but the video

images of the responses to the WN and FM sounds (Fig. 4.1A) show differences in the

areas that were activated within the same field of view.
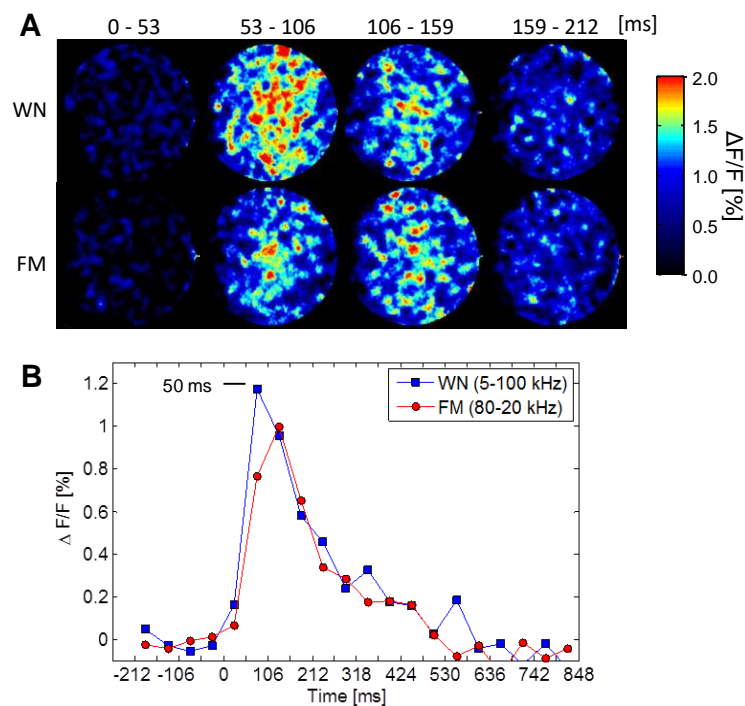
Figure 4.1 Optically recorded neuronal responses in bat's IC
(A) Series of four successive averaged video frames of optical responses from IC for stimulation by WN (top) and FM (bottom). Response decays substantially over first 2 frames. **(B)** Plot of averaged optical response (*ΔF/F*) for full series of images.

4.3.2 *Intensity-dependent changes and spatial difference in single viewfield*

To examine the intensity-dependent changes in the calcium responses in bats, we systematically changed the SPL from 40 dB to 90 dB. Significant responses were observed above 40 dB and 70 dB to the WN and FM sounds, respectively (Fig. 4.2). The Ca^{2+} fluorescence results indicated that responses differed for different SPLs. The Ca^{2+} responses to the WN initially increased with SPL increases, reaching a maximum at 60 dB, and subsequently decreased at higher SPLs (Fig. 4.2). In contrast, the Ca^{2+} responses to the FM sounds increased steadily with the SPL increases (Fig. 4.2). We also found spots that had sizes that corresponded to the sizes of IC neurons (Fig. 4.3A). By separately analyzing the individual spots, we detected independent response properties to changes in SPL for each spot (Figs. 4.3B and C).
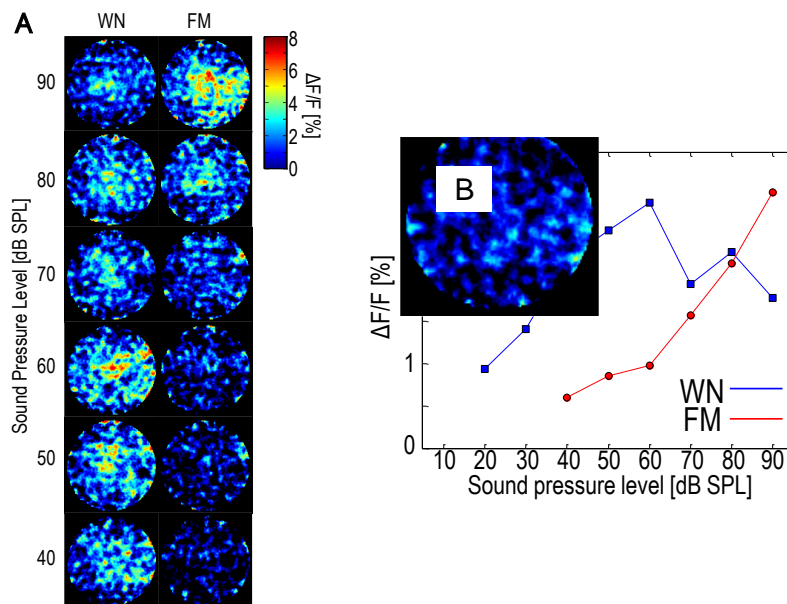
Figure 4.2 Dependence of sound pressure level for Ca²⁺ response
(A) Micro-endoscopic images of the stimulus frame (left column, 0 - 53 ms, 5th frame) and the peak frame (right column, 53 - 106 ms, 6th frame) of Ca²⁺ (optical) response (*ΔF/F*) to several sound intensities. Field of view = 300 μm. Sound (white noise) was applied during 5th frame. **(B)** Sound level dependence of averaged Ca²⁺ responses to WN (blue) and FM (red).
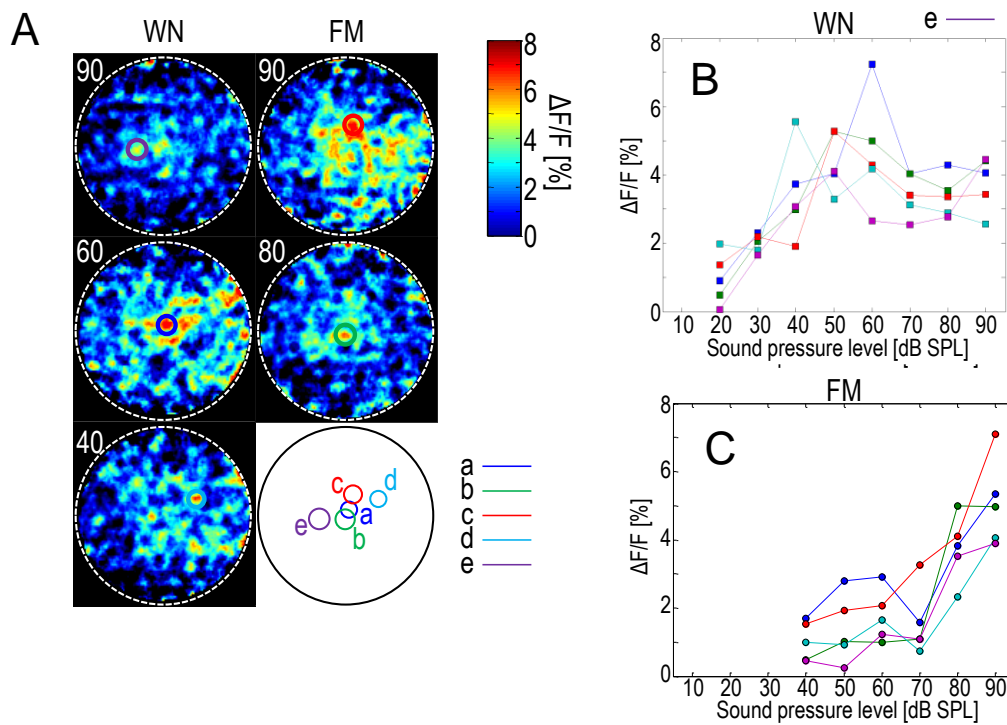
Figure 4.3 Spatial difference of calcium responses in single viewfield
(A) Five hot spots (a - e) observed in one endoscopic viewfield are circled. Field of view = 300 μm. **(B)** Sound level dependence of Ca^{2+} responses corresponding to five areas labeled in Fig. 4.3B.

4.4 Discussion

The calcium imaging in the experiments on the bats was able to be performed with almost the same procedures as those on the mice, except for the incubation time. However, unlike in the mouse IC, it was difficult to stain the cells with OGB in the bat IC. Although the cell bodies were labeled in some cases like in the mice, the bat neurons were never labeled and could not be identified. Although fluorescence changes that corresponded to the size of the IC neurons were observed, as shown in Fig. 4.3, it was unclear whether they were cell bodies. Thus, methods that label cell bodies, such as fluorescent proteins, are required to identify the cell bodies and elucidate the neural networks.

In addition, the peak frames of the calcium responses differed between the WN and FM sweeps. The peak frame of the calcium response against WN was the fifth frame, whereas the $\Delta F/F$ evoked by the FM sweeps peaked in the sixth frame (Fig. 4.1). Although the onsets of these sound stimuli were the same, the peak frame differences were thought to be due to the differences in their frequency structure. However, because the time resolution of optical measurements is insufficient to determine the specific time difference between these responses, it is necessary to compare the electrical activities of these responses.

4.5 Summary

Optical recordings were conducted in the bat IC using the micro-endoscopic system and the recording procedures established in the mice experiments. We optically recorded calcium responses to the WN and FM sounds and detected hot spots with sizes that corresponded to the size of the IC neurons. Thus, we established an optical recording method that can be used in bats. However, we did not examine electrical activity in these experiments in bats even though electrophysiological recordings are much easier to perform using this micro-endoscope than optical recordings are, as described in Chapter 3. Thus, we can use this method to optically and electrically record neural activity during bat echolocation.

CHAPTER 5.

Multiple Timescales of Auditory Responses in the Inferior Colliculi of Two Species of Echolocating Bats

5.1 Introduction

In the bat auditory pathway, the IC is the predominant center for the integration of information about echo delay from the timing (latency) of spikes with information about echo spectra from the frequency tuning of the neurons (Covey and Casseday, 1995). The IC is tonotopically organized from low to high frequency by depth, whereas latencies cover a span from approximately 5 to 50 ms, which is regulated by intracellular inhibition that is graded in duration across different neurons (Covey et al., 1996). Although electrophysiological recordings contain sharp peaks that have temporal resolution in fractions of milliseconds, the associated latency-determining intracellular inhibition is graded more coarsely, rising and falling over milliseconds and tens of milliseconds. Thus, two very different timescales are manifested in the response properties of the neurons in the bat IC. Besides temporal resolution, the information that is conveyed by the spatial patterns of the response timings across many cells in the bat IC is not known. To examine the spatial dimensions of the responses across neural tissue, we developed the micro-endoscope system described above. We investigated whether the optical responses conformed to the fast timescale of the electrophysiological recordings or the slow timescale of intracellular inhibition.

In this chapter, we describe experiments in which we tested the hypothesis that optical signals are faster than the video frame rate using line-scan recordings from the IC of two species of FM echolocating bats (big brown bat, *E. fuscus*, and short-tailed fruit bat, *C. perspicillata*).

5.2 Materials and Methods

5.2.1 *Animals*

The subjects were two species of FM echolocating bats, 5 big brown bats (*E. fuscus*) and 8 short-tailed fruit bats (*C. perspicillata*). Mixed anesthetic (Medetomidine: 0.4 mg/kg, Midazolam: 4.0 mg/kg, Fentanyl: 0.4 mg/kg) was injected into the bat intraperitoneally. The anesthetized bat was then placed on an aluminum platform, wrapped in cotton gauze with a hand warmer (Iris Oyama Co, Sendai, Japan) placed on its back to maintain body temperature in the range of 25–30 ºC. After removing fur and skin of their head, the medial tendon (origin point) of temporal muscle was cut and pushed to lateral direction to expose the skull. Then, a craniotomy was performed over the inferior colliculus (IC). In case of *C. perspicillata*, since their IC was covered with transverse sinus (TS) and the cerebellum (Cb), we pushed away TS and Cb to caudal and rostral directions respectively to expose the IC. All protocols were approved by the Animal Research Committee of Brown University.

5.2.2 *Acoustic stimuli*

Sound stimuli were tone bursts of constant frequency (CF: 10, 20, 40, 60 and 80 kHz), downward frequency modulated sounds (FM1: 100–30 kHz and FM2: 80–20 kHz), and white noise bursts (WN: 5–100 kHz). The sound duration was 50 ms including 1 ms rise and fall times with raised cosine slope. Sound pressure level was varied from 10 to 90 dB SPL (re: 20 µPa) in 10 dB steps. Stimulus sound was created by playing the waveform, which was computed online using MATLAB (MathWorks, Natick, MA, USA), through a 16 bit D/A converter (NI PCI-6259, National Instruments, Austin, TX, USA) at a sampling rate of 200 kHz. These acoustic stimuli were presented from a loud speaker in a sound-attenuated chamber. The distance between the speaker and the animal was set at 25 cm. The sound stimuli were periodically presented at approximately 1 Hz (every 20 frames) while recording.

5.2.3 *Loading of Ca^{2+} sensitive fluorescence indicator dyes*

Oregon green 488 BAPTA-1, AM (OGB, Thermo Fisher Scientific, Waltham, MA, USA) was diluted with saline to be 0.8 mM and loaded into a glass micro-pipette, which was fabricated using a puller (PE-2, Narishige, Tokyo, Japan). OGB solution (1.0 µL) was injected by air pressure into the IC at depths of 250, 650, and 1,050 µm from the dorsal brain surface.

5.2.4 *Electrophysiological recordings*

The micro-endoscope was inserted into the IC after dye incubation for 60 min. The depth of the tip was controlled using a motorized micromanipulator (SM-191; Narishige Co., Ltd., Tokyo, Japan). The tip was coated with gold using a sputter coater (IB-3, Eiko Engineering Co., Ltd., Ibaraki, Japan) and subsequently coated with silver (Leitsilber 200 Silver Paint; Ted Pella, Inc., Redding, CA, USA) and enamel paint (TPU F2-26NC; Tohtoku, Tokyo, Japan) so it could be used as a recording electrode. The electrical signals that were recorded from the edges of the micro-endoscope tip were impedance-converted using a bridge amplifier, bandpass filtered (1–6 kHz), and subsequently transferred and stored on a PC using an A/D converter (NI PCI-6259; National Instruments, Austin, TX, USA) at a sampling rate of 20 kHz. The electrical signals were separated into LFPs (4–50 Hz) and MUAs (300–3,000 Hz) using a digital filter in MATLAB.

5.2.5 *Optical recordings: image scanning and processing*

The laser scanner in the micro-endoscope is composed of two mirrors, as shown in the diagram in Fig. 5.1B. Each mirror axes correspond to the X-axis (vertical axis) and Y-axis (horizontal axis) of the micro-endoscopic images. One of the mirrors (X-scanner) is a resonant galvano scanner (CRS 4 kHz; Cambridge Technology, Bedford, MA, USA), which controls the X-axis scanning. The other mirror (Y-scanner) is a galvanometer scanner (G120; Cambridge Technology), which scans the Y-axis. The angle of the Y axis is controlled with the input voltage signal shown in Figs. 5.1C and D. In a normal-scan, the input signal is a sawtooth wave used to scan the fiber bundle surface from top to bottom (Fig. 5.1E). Because the sawtooth wave cycle is 53 ms, a

normal-scan takes 53 ms to obtain a one-frame endoscopic image. In contrast, the input signal in a line-scan is a predetermined constant voltage that fixes the Y-scanner angle (Figs. 5.1D and E). A line-scan can scan one line for 53 ms. Thus, a normal-scan is limited to 18.9 frames/s (53 ms/frame) by the scanning mirror (Fig. 5.1F), whereas a line-scan yields 7,550 lines/s or 132 µs for one line (Fig. 5.1G). In addition, we were able to acquire any scanning line image by changing the Y-scanner angle (input voltage signal) during the line-scan (Fig. 5.1H). The details on how to acquire and process endoscopic images in normal-scans are described in our previous report (Yashiro et al., 2017a). For normal-scans, the average value of the optical responses was calculated with MATLAB using 20 frames as one period, and *ΔF/F* was calculated using the baseline of the average value of the four frames recorded before the sound stimulation. For line-scans, micro-endoscopic images were acquired and processed in the same way as the normal-scans. To calculate *ΔF/F* in a line-scan, the average fluorescence of the 1,600 lines (the four frames in a normal-scan) recorded before the sound presentation was subtracted from the fluorescence obtained in each line during and after the sound presentation.
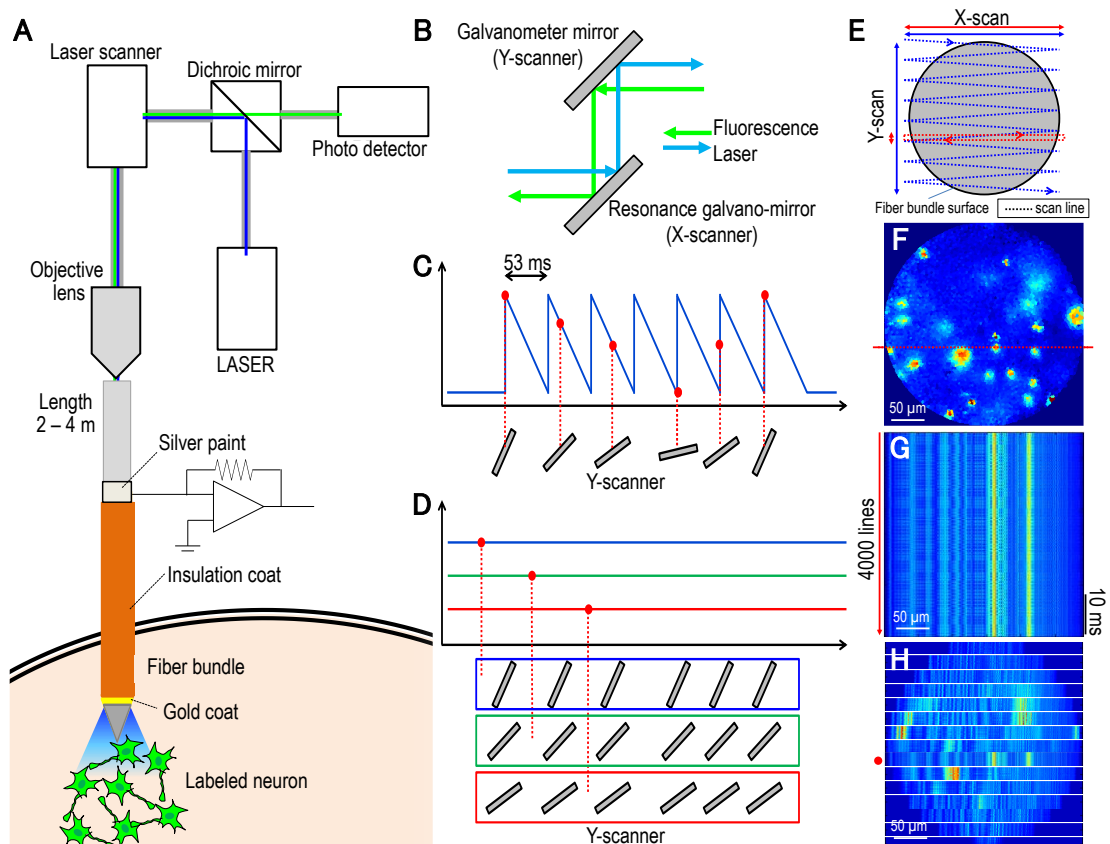
Figure 5.1 The micro-endoscope system for simultaneous optical and electrical recordings

Schematic drawings of the **(A)** micro-endoscope system, **(B)** scanning mirrors, **(C)** input signals to the scanning mirror controlling the Y-scanner in a normal-scan, and **(D)** a line-scan. **(E)** Normal-scan video image of endoscope fiber bundle (blue) and single repetitive horizontal line-scan to obtain line image in 132 µs (red). Each frame time of normal-scan video is 53 ms. **(F)** A representative full video frame image (normal-scanned image). The sites of optical responses are shown in red and yellow. **(G)** Series of line images from one recording (traced by the red dashed line in F). **(H)** An example of the combination of the line-scan images. The image indicated by the red dot is the same image as the one in Fig. 5.1G.

5.2.6 *Experimental Design*

Sixty min after the dye injections, the fiber tip was positioned on the surface of the IC. The prestimuli were presented at a rate of approximately 1 Hz (every 20 frames) to allow observation of the sites of fluorescence changes. To increase the synchronization of the neural activities, 90-dB WN bursts were used as the prestimulus because the fluorescence intensity of OGB has been reported to increase proportionally with the number of spikes (Ikegaya et al., 2005). Although the changes in fluorescence were sometimes confirmed without averaging in our previous experiment conducted in mice, the changes could not be seen without averaging in the bats. For this reason, we advanced the endoscope tip by 50-μm steps from the surface of the IC to a depth of approximately 1,500 μm and examined whether the changes in fluorescence could be confirmed at each depth. If changes in fluorescence were seen in the averaged data for approximately 30 to 40 s while the prestimulus was presented every 20 frames, the measurements were started at that depth.

In the mouse experiments, 30 s was sufficient to record clear optical and electrical responses to one sound condition (Yashiro et al., 2017a). Hence, the recording time for each condition was set to 30 s in the bats. The data recorded during the 30 s can be calculated by averaging the data of each second 27 times. Usually, 558 frames are included in the 30 s of data, and we only used the first 540 frames to calculate the averaged 20 frames (averaged fluorescence: F). Subsequently, the average fluorescence of the first 4 frames in F was subtracted from the fluorescence obtained in each frame to determine the fluorescence change from baseline (ΔF) and the fractional change in fluorescence ($\Delta F/F$). To perform these processes, we wrote MATLAB codes (The MathWorks, Inc., Natick, MA, USA) so that we could confirm

the auditory responses immediately after the recordings. However, the process took approximately 1 min during the mouse measurements (Yashiro et al., 2017a). We therefore rewrote the codes so that the required processing could be done in approximately 10 s. Consequently, the recording time needed for one sound stimulus was greatly shortened. The stimulus was presented at the SPL of the sound stimulation at 90 dB and subsequently decreased in 10-dB steps. If a response was not observed, we used the other sound stimulus and presented at 90 dB again. Because OGB did not work in regions deeper than approximately 1,500 μm, the endoscope tip was withdrawn and inserted into another IC region after recording at the deepest area. Optical measurements were subsequently conducted again in the same way.

Electrophysiological data were recorded simultaneously with optical measurement. While electrophysiological activities were enough S/N ratios even without averaging, we calculated these into 27 times averaging of 1 s data because the data lengths were also 30 s. These raw data were separated into LFPs and MUA using MATLAB.

Figure 5.2 Calcium responses recorded by normal-scan and line-scans
(A) Series of averaged full video images for comparison with **(B)** series of line-scan images. **(C)** Plot showing the time course of *ΔF/F* for the discrete full images (squares) and line-scans (continuous curve). **(D)** Average peak latency of the calcium responses recorded from *Carollia perspicillata* (blue lines) and *Eptesicus fuscus* (red lines). The error bars indicate standard deviations.

5.3 Results

5.3.1 *Calcium responses recorded by normal-scan and line-scan*

Because it is difficult to compare electrical activities and calcium responses in the normal-scan data, we attempted to perform line-scans for the image acquisition during the recording in order to improve the time resolution of the optical measurements. The $\Delta F/F$ results for the recordings made with normal- and line-scans are compared in Fig. 5.2. Eight frames (424 ms) of normal-scanned images are shown in Fig. 5.2A, and pseudo colored $\Delta F/F$ data that were determined with line scans are shown in Fig. 5.2B in the same time range as the images shown in Fig. 5.2A. The average values of the calcium responses in Figs. 5.2A and B are plotted in Fig. 5.2C. The square marker and dotted line are the normal-scanned $\Delta F/F$, and the solid curve is the mean value of the calcium responses recorded by the line-scans. Even though the approximate shapes did not significantly change, the line-scans enabled us to measure more detailed time changes of the calcium responses. The latencies of the maximum values of the changes in fluorescence that were measured by line-scans are plotted for each kind of bat and sound stimulus type (Fig. 5.2D). These methods made it possible to measure the differences in the latencies of each response in the different conditions.

To examine the sound duration-dependent changes in the calcium responses, the SPL was fixed at 90 dB SPL, and the durations of the sound stimuli were changed to 5, 20, and 50 ms. Figs. 5.3 and 5.4 show the result for LFP, MUA, and $\Delta F/F$. The response times of the calcium responses were longer as the sound stimulus lengths increased. The response duration and amplitude elongated and increased according to the sound duration, whereas the rising timing and inclination seemed to be almost the same for

every duration. In contrast, the results of the SPL-dependent changes are shown in Figs. 5.3 and 5.4. The amplitudes and rising inclinations differed, whereas the peak latencies appeared constant at all SPLs. These results showed that detailed measurements of the time courses of the calcium responses were possible using line-scans.
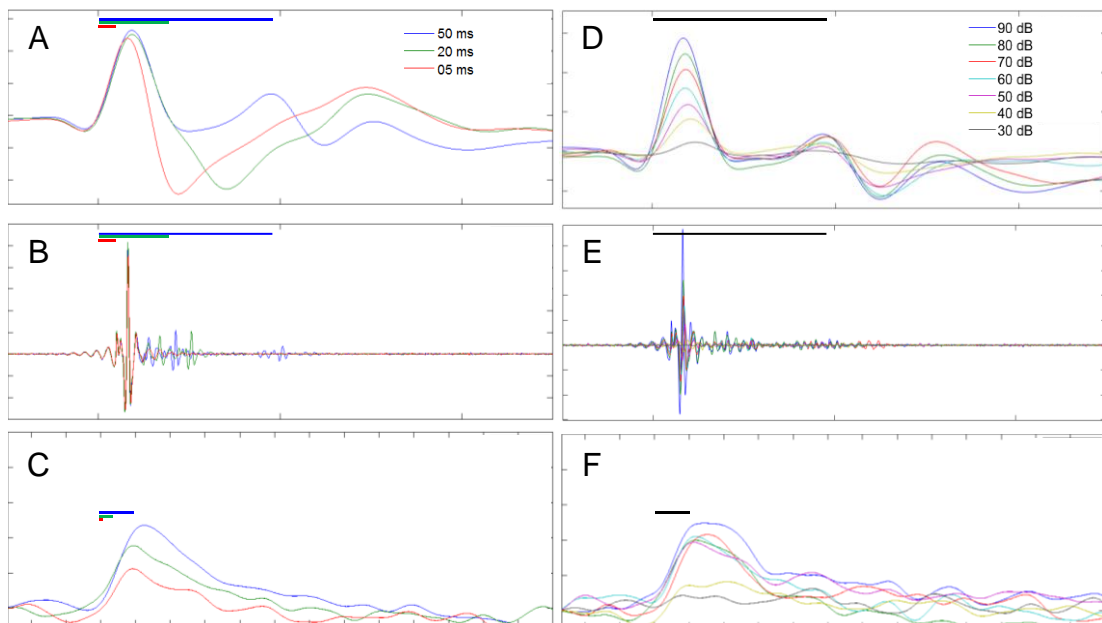
Figure 5.3 Dependence on sound pressure level and sound duration
(A), (D) Plots showing the time courses of the local field potentials. **(B), (E)** Multiunit activity. **(C), (F)** *ΔF/F* evoked by white noise. Horizontal bars show the sound stimuli.
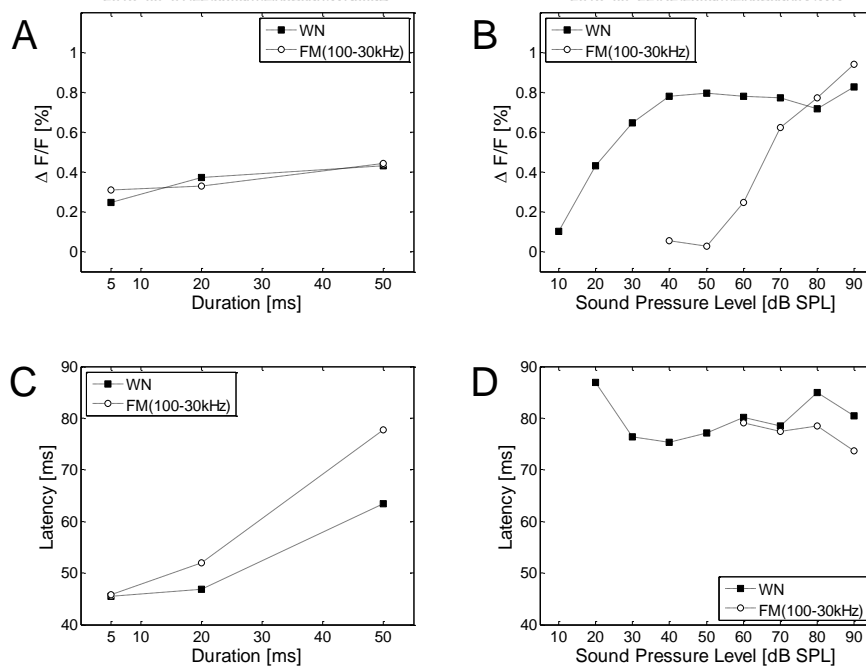
Figure 5.4 Level and duration functions of the calcium responses
(A) The amplitude-duration function and **(B)** amplitude-level function of the calcium responses to white noise (WN) and frequency modulation (FM). **(C)** The latency-duration function and **(D)** latency-level function of the calcium responses to WN and FM.

5.3.2 *Spatial resolution of line-scan*

Because the line-scans lowered the spatial resolution instead of improving the temporal resolution, we therefore investigated whether differences in the spatial auditory responses can be confirmed on a single scanned line. The *ΔF/F* results for the recordings made during the 200 ms after the onset of several frequencies of sounds (WN and CF: 10, 20, 40, 60, and 80 kHz) in *C. perspicillata* by line-scans are shown in Fig. 5.5A. The recordings were performed at four recording depths (350, 500, 650, and 850 μm). Fluorescent changes were evoked at every depth by WN, whereas the response to 80 kHz appeared only at 650 and 850 μm. The mean values of the activated areas (yellow and red area) are shown in Fig. 5.5B. Comparisons of these results show that the responses to the high frequencies increased as the recording depth got deeper.

Fig. 5.5C shows plots of the calcium responses to WN at 500 μm at the positions indicated by the red, blue, and green arrows (a, b, and c, respectively) shown in Fig. 5.5A. Differences in the *ΔF/F* onset and number of peaks are visible. Thus, changes in spatiotemporal calcium fluorescence can be recorded, even with line-scans.
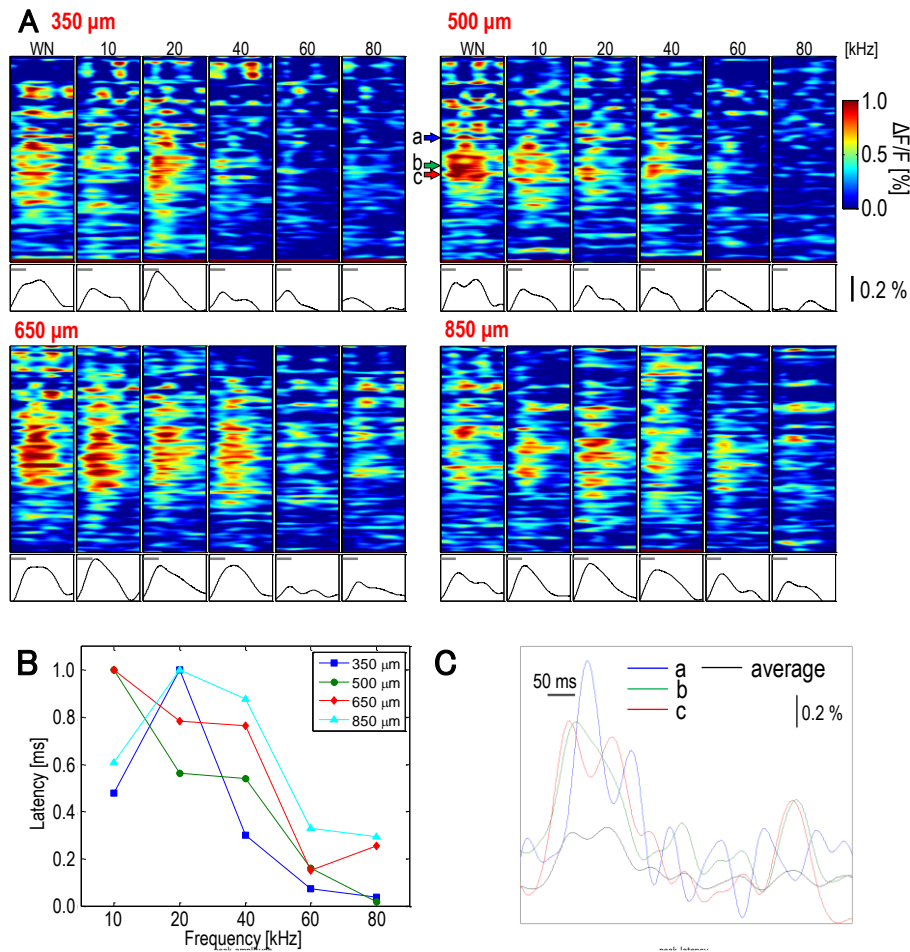
Figure 5.5 Calcium responses to tone bursts with constant frequencies recorded with line-scans

(A) Pseudo colored line-scan images and time courses of the average *ΔF/F* of the image (0–200 ms from the stimulus onset). The sound stimuli were 90-dB sound pressure level (SPL) noise bursts (5–100 kHz) and tone bursts (10, 20, 40, 60, and 80 kHz) with a 50 ms duration (the gray horizontal lines indicate the stimulus). The recording depths in the inferior colliculus are written in the bottom-right corner of each color map. **(B)** The frequency-dependent changes in the areas of activation (red and yellow hot spots area in A). The number of pixels in the activated area was normalized by dividing it by the maximum value in each condition. **(C)** Plot of the time courses of the hot spots in Fig. 5.5A.

5.3.3 *Neuronal electrical activities recorded from fiber edge electrode*

The results of the electrophysiological recordings are shown in Fig. 5.6. Waveforms for the LFPs and MUAs evoked by WN (90–10 dB SPL) are shown in Figs. 5.6A and B, respectively. These waveforms were converted into a waterfall plot with a heat map, and the color map on the right side indicates the pseudo colors of amplitude (Figs. 5.6C and D). Both LFP and MUA were evoked by the sound stimulation immediately after its onset, and the latencies were elongated as the SPL decreased. For the MUAs, the responses seemed to correspond to the length of the duration of the sound stimulus, but the peak occurred immediately after the sound onset. In addition, before 10 ms, the latency changed according to the SPL, but it did not change between 10 and 60 ms. In contrast, the LFPs had a bimodal peak (red area), and inhibitory responses were observed after the sound offset (blue area).
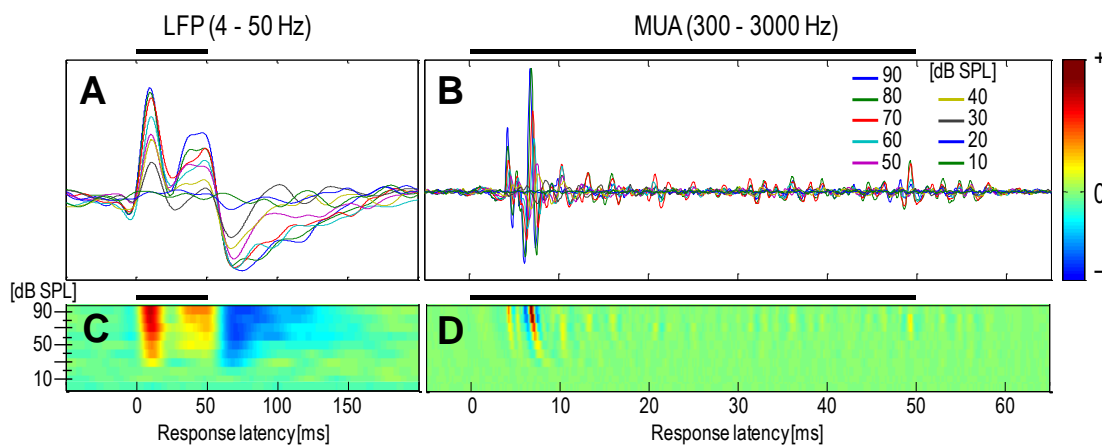
Figure 5.6 Electrophysiological activities evoked in bat's IC
(A), **(C)** Heat map of IC multi-unit activities filtered from 300 to 3000 Hz to capture rapid events such as spikes. **(B)**, **(D)** Heat map of IC evoked potentials filtered from 4 to 50 Hz. Horizontal axis shows response latency from noise-burst onset (black horizontal lines show stimulus). Plots show heat maps of response amplitude (red +v, blue -v) at different stimulus levels. Vertical axis shows stimulus level from 90 dB SPL down to 10 dB SPL in 10 dB steps.

5.4 Discussion

5.4.1 *Detailed time course of calcium responses*

Because of the improved temporal resolution, it became possible to record the detailed time course of the changes in calcium fluorescence. The recordings of the changes in fluorescence that occurred in response to the different durations of the stimuli showed that the time lengths and peak latencies of the calcium responses changed according to the changes in sound duration (Figs. 5.3 and 5.4). In contrast, no significant differences were observed between the peak latencies and durations of the calcium responses when the SPLs changed, even though the amplitudes varied (Fig. 5.3). Although the rising slope of the calcium response did not change when the duration of the stimulus changed, the rising inclination increased as the SPL increased. Hence, the rising inclination of the response was influenced by increase of the sound stimulus. The synchronization rate of neural firing has been reported to be enhanced by steep increases in the sound stimulus (Davis and Zerlin, 1966; Onishi and Davis, 1968). Previous observations that the intensity of the fluorescence of OGB changes according to the number of spikes (Ikegaya et al., 2005) suggest that the changes in the calcium response were influenced by the changes in the rising inclination and duration of the sound stimuli

5.4.2 *Frequency- and depth-dependent changes in the calcium responses*

Comparisons of the activated areas in Fig. 5.5A (yellow and red areas) with the strong changes in the fluorescence at each recording depth showed that the responses to the high frequencies became stronger as the recording depth got deeper (Fig. 5.5B). In contrast, the responses to 20 kHz showed robust responses at any depth. These characteristics have also been reported in electrophysiological experiments, which suggests that the neurons with best frequencies approximately 20 kHz are found at every depth (Goto et al., 2010). These results showed that, even if the scanning method was changed, differences in the depth direction could be recorded and that the tonotopic organization was confirmed in the IC.

5.4.3 *Spatial resolution of the line-scanned image*

The spatial information of the line-scanned images was considerably inferior to the normal-scanned images, but the spatial changes could be seen even within only one scanned line. Fig. 5.5C shows that the changes in fluorescence differed on the same scanned line, and spatially different responses can be observed at other depths and frequencies in Fig. 5.5A. In addition, Fig. 5.1H, which is a combination of line-scan images, shows the approximate positional relationship of the fluorescent beads, even though the resolution is inferior to that of Fig. 5.1F. These results suggested that performing line-scans many times might compensate for the low spatial resolution. By recording the detailed time courses of the changes in fluorescence with line-scans after recording the activities of the entire viewfield with normal-scans, responses that

cannot be recorded with normal-scans alone can be recorded, as shown in Fig. 5.5. Thus, the combination of normal- and line-scans complement each other's disadvantages and improve the ability to elucidate the cranial nerve network.
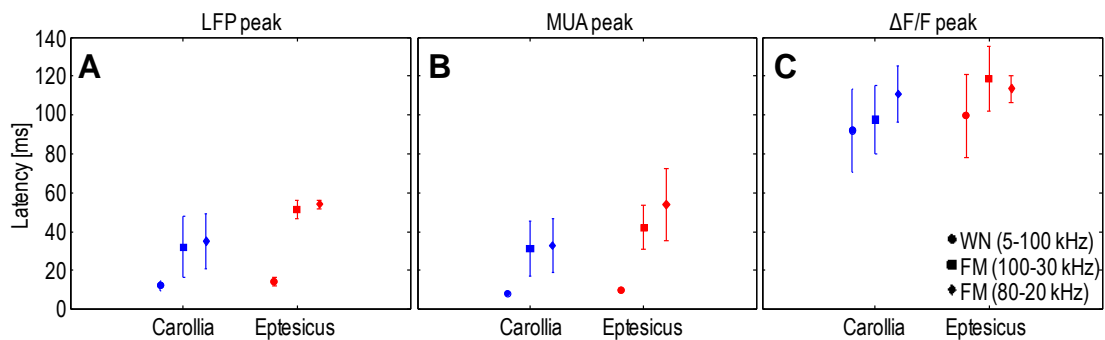
Figure 5.7 Peak latencies of Ca²⁺ responses and electrophysiological activities
(A) Average Peak latency of MUA, **(B)** LFP and **(C)** calcium responses recorded from Carollia perspicillata (blue plots) and Eptesicus fuscus (red plots). Error bars show the standard deviation.
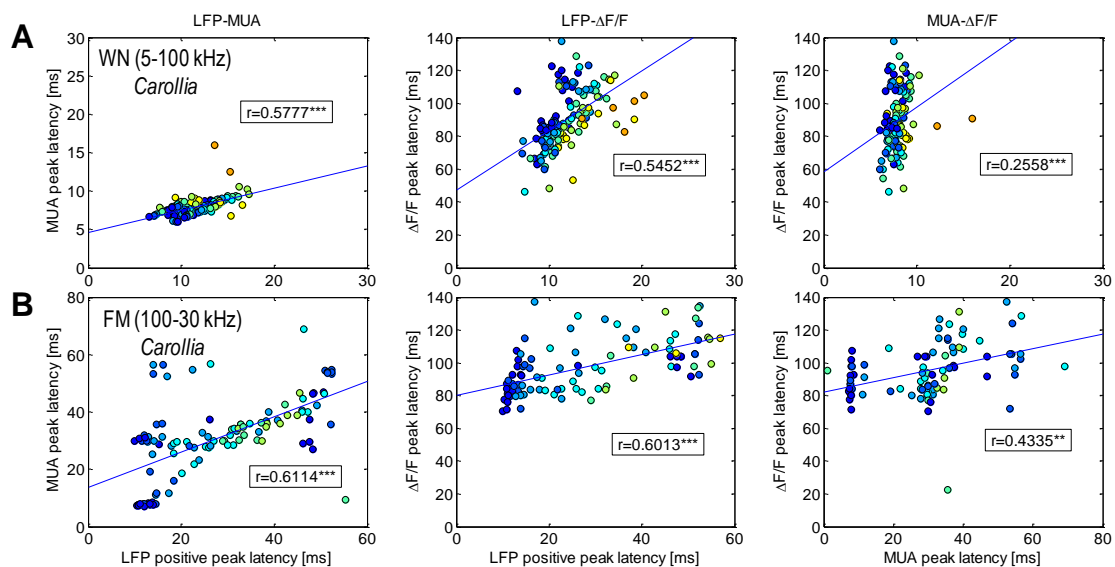
Figure 5.8 Comparisons of the electrical activities and calcium responses
(A) Scatter diagram of the peak latencies of the responses to a noise burst. The blue lines approximate the scatter plots by the least square method. The correlation coefficient of the scatter plot is written with asterisks: ** p < 0.01, *** p < 0.001. The sound pressure levels of the sound stimuli are represented by the marker color according to the color scale bar. **(B)** Scatter diagram of the peak latencies of the responses to the frequency modulation sound sweeps (100–30 kHz).

5.4.4 *Spatial resolution of the line-scanned image*

Fig. 5.7 show the peak latencies of the LFPs, MUAs, and *ΔF/F* in response to WN, FM1, and FM2, respectively, that were recorded from two species of bat [C. perspicillata (blue) and E. fuscus (red)]. The calcium and electrophysiological responses differed by over 60 ms. We therefore investigated the correlations among LFP, MUA, and *ΔF/F* to examine the relationship between calcium and electrophysiological responses. These results showed that LFP was positively correlated with both MUA and *ΔF/F* (Fig. 5.8).

5.5 Summary

We were able to improve the time resolution of the micro-endoscope by restricting the range of the scanned area. As a result, the temporal resolution increased up to 7,550 lines/s, and the detailed time courses of the changes in the calcium response that were evoked by various types of sound stimuli could be recorded. The calcium responses recorded from the two species of FM echolocating bats (big brown bat, *E. fuscus*, and short-tailed fruit bat, *C. perspicillata*) showed that the peak latencies were much slower (more than 60 ms) than that of the electrophysiological responses (LFPs and MUAs). However, the electrical activities and calcium responses had specific correlations (LFP and *ΔF/F*). Therefore, these results suggested that, even though it is impossible to compare electrical activity and calcium responses in a simple way, it is expected that these relationships can be clarified by conducting simultaneous recordings with our micro-endoscope. As described above, we believe that combining the recordings of optical and electrophysiological responses can lead to elucidation of neural networks.

CHAPTER 6.

Optical and Electrical Responses Evoked by Mimic Pulse and Echoes in FM Echolocating Bats

6.1 Introduction

 Insectivorous bats use echolocation to orient and guide flight in their surroundings (Neuweiler, 2000b). Most species transmit trains of brief, frequency-modulated (FM) sounds and exploit the signals' wide bandwidth for perceiving objects as acoustically-derived images (Simmons, 2012). The distance to reflecting objects, such as insect prey, is determined from the time delay between outgoing biosonar broadcasts and returning echoes, while the distinguishing features of object shape and size are determined from comparison of echo spectra with broadcast spectra (Simmons et al., 1995; Simmons, 2012). The bat IC contains CSNs that are tuned to detect specific time differences between pulses and echoes (Wenstrup et al., 2012; Suga, 2015). Other than the IC, CSNs are also found in the MGB and AC, which are higher brain regions compared with the IC (Suga et al., 1983; Olsen and Suga, 1991; Wenstrup et al., 2012; Suga, 2015). Previous studies have reported that basic local circuits create CSNs in the IC by receiving various types of projections (Wenstrup et al., 2012; Suga, 2015). Recording optical and electrophysiological responses simultaneously using our micro-endoscope might result in the clarification of this neural network. However, as shown in Chapter 5, the calcium responses did not seem to follow the electrophysiological changes on the order of milliseconds. However, perhaps specific calcium responses might be seen in the CSNs

that respond to the time differences of the mimic pulses and echo sounds that simulate the sounds used during echo location.

In this chapter, we describe the results of the experiment in which we used line-scans to record optical signals in the IC that occurred in response to mimic pulses and echoes in FM echolocating bats (big brown bat, *E. fuscus*).

6.2 Materials and Methods

6.2.1 *Animals*

The subjects were 3 big brown bats (*E. fuscus*). Mixed anesthetic (Medetomidine: 0.4 mg/kg, Midazolam: 4.0 mg/kg, Fentanyl: 0.4 mg/kg) was injected into the bat intraperitoneally. The anesthetized bat was then placed on an aluminum platform, wrapped in cotton gauze with a hand warmer (Iris Oyama Co, Sendai, Japan) placed on its back to maintain body temperature in the range of 25–30 °C. After removing fur and skin of their head, the medial tendon (origin point) of temporal muscle was cut and pushed to lateral direction to expose the skull. Then, a craniotomy was performed over the inferior colliculus (IC). All protocols were approved by the Animal Research Committee of Brown University.

6.2.2 *Acoustic stimuli*

Sound stimuli were two harmonics down ward frequency modulated sounds (1st harmonic: 50–20 kHz, 2nd harmonic: 100–40 kHz, Fig. 6.1A). The sound duration

was 3 ms including 1 ms rise and fall times with raised cosine slope. To mimic bat echolocating sounds (pulse and echoes), the FM sweep (mimic pulse) was presented first at 90 dB SPL and accompanied with attenuated FM sweeps (mimic echoes) after some time delay (2–12 ms in 2 ms steps or 0–100 ms in 5 ms steps). The number of echoes was 1 or 5 (Figs. 6.1B and C). The mimic echoes were varied from 40 to 80 dB SPL (re: 20 µPa) in 10 dB steps. Stimulus sound was created by playing the waveform, which was computed online using MATLAB (MathWorks, Natick, MA, USA), through a 16 bit D/A converter (NI PCI-6259, National Instruments, Austin, TX, USA) at a sampling rate of 200 kHz. These acoustic stimuli were presented from a loud speaker in a sound-attenuated chamber. The distance between the speaker and the animal was set at 25 cm. The sound stimuli were periodically presented at approximately 1 Hz (every 20 frames) while recording.

Figure 6.1 Mimic pulses and echoes
(A) Spectrogram of the mimic pulse sounds showing two downward harmonics to the frequency-modulated sounds (1st harmonic: 50–20 kHz; 2nd harmonic: 100–40 kHz). (B) Spectrogram of the mimic pulses and echoes or (C) series of echoes. The mimic echoes were attenuated. The time delay of the echo sound was changed from 2 to 12 ms, and the interecho intervals were fixed to 3 ms.
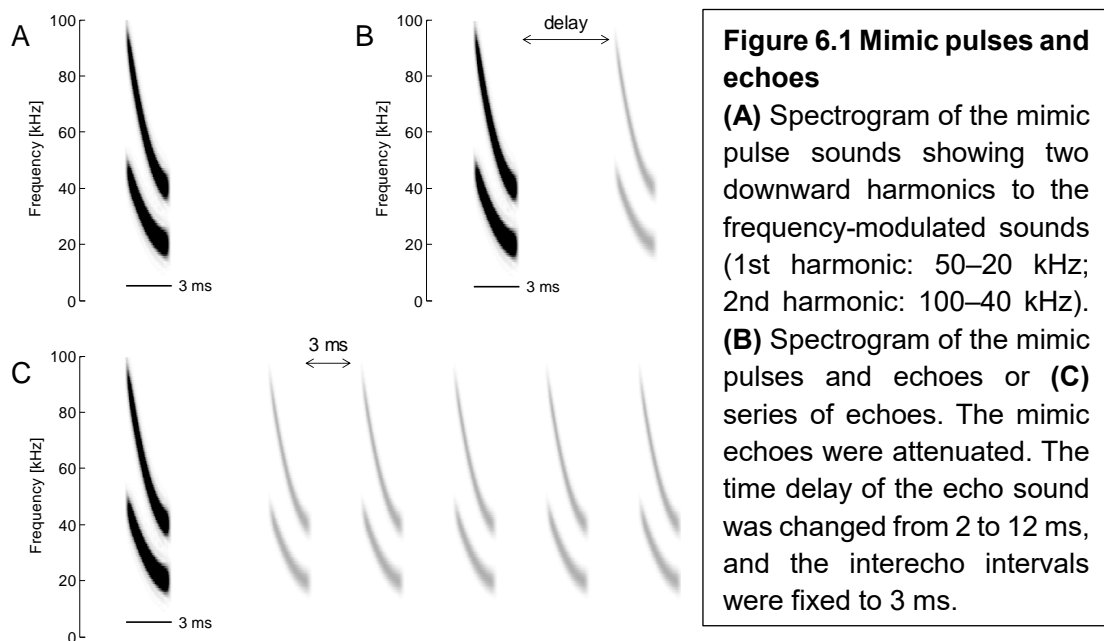
6.2.3 *Electrophysiological recording and Optical recording*

The micro-endoscope was inserted into the IC after dye incubation for 60 min. The depth adjusting of the tip was controlled by a motorized micro-manipulator (SM-191, Narishige, Tokyo, Japan). The tip was coated with gold using a sputter coater (IB-3, Eiko, Ibaraki, Japan), and then coated with silver paint (Leitesilber 200 Silver Paint, Ted Pella Inc., Redding, CA, USA) and enamel paint (TPU F2-26NC, Tohtoku, Tokyo, Japan) to be used for a recording electrode. Electrical signals recorded from the edges of the micro-endoscope tip were impedance-converted using a bridge amplifier, band-pass filtered (1–6 kHz) and stored on a PC through an A/D converter (PCI-6259, National Instruments, Austin, TX, USA) at a sampling rate of 20 kHz. Electrical signals were separated into local field potential (LFP: 4–300 Hz) and Multi-unit activities (MUA: 300–3000 Hz) using a digital filter in MATLAB.

6.2.4 *Experimental Design*

Sixty min after the dye injections, the fiber tip was positioned on the surface of the IC. The prestimuli were presented at a rate of approximately 1 Hz (every 20 frames) to allow observation of the sites of fluorescence changes. To increase the synchronization of the neural activities, 90-dB WN bursts were used as the prestimulus because the fluorescence intensity of OGB has been reported to increase proportionally with the number of spikes (Ikegaya et al., 2005). Although the changes in fluorescence were sometimes confirmed without averaging in our previous experiment conducted in mice, the changes could not be seen without averaging in

the bats. For this reason, we advanced the endoscope tip by 50-μm steps from the surface of the IC to a depth of approximately 1,500 μm and examined whether the changes in fluorescence could be confirmed at each depth. If changes in fluorescence were seen in the averaged data for approximately 30 to 40 s while the prestimulus was presented every 20 frames, the measurements were started at that depth.

In the mouse experiments, 30 s was sufficient to record clear optical and electrical responses to one sound condition (Yashiro et al., 2017a). Hence, the recording time for each condition was set to 30 s in the bats. The data recorded during the 30 s can be calculated by averaging the data of each second 27 times. Usually, 558 frames are included in the 30 s of data, and we only used the first 540 frames to calculate the averaged 20 frames (averaged fluorescence: F). Subsequently, the average fluorescence of the first 4 frames in F was subtracted from the fluorescence obtained in each frame to determine the fluorescence change from baseline ($\varDelta F$) and the fractional change in fluorescence ($\varDelta F/F$). To perform these processes, we wrote MATLAB codes (The MathWorks, Inc., Natick, MA, USA) so that we could confirm the auditory responses immediately after the recordings.

The sound pressure level of mimic pulse was set to 90 dB SPL constantly, and that of mimic echoes was attenuated from 80 to 40 dB SPL in 10 dB steps. First, we presented one 90 dB pulse as a stimulus. Then, pulse and 80 dB echo (or 5 echoes) were presented. After presenting pulse and 40 dB echo, we changed the recording sight. Since OGB was not worked in regions deeper than about 1,500 μm, the endoscope tip was drawn and inserted into the other IC after the recording at the deepest area. Then, optical measurements were conducted in the same way again.

Electrophysiological data were recorded simultaneously with optical measurement. While electrophysiological activities were enough S/N ratios even without averaging, we calculated these into 27 times averaging of 1 s data because the data lengths were also 30 s. These raw data were separated into LFPs and MUA using MATLAB.
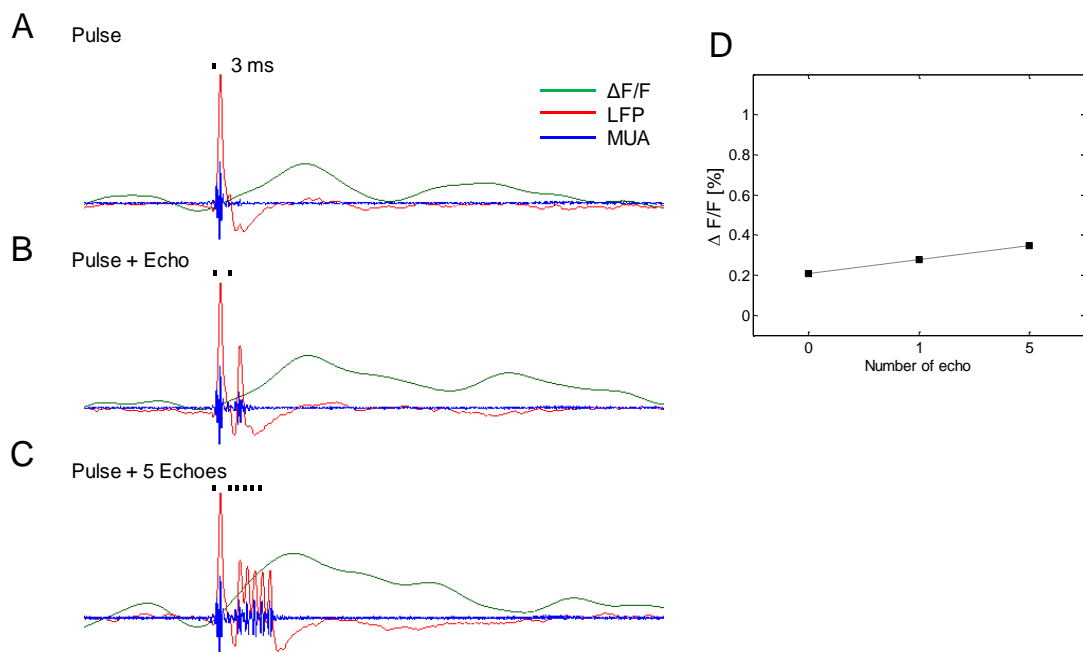
Figure 6.2 Optically and electrically recorded neuronal responses
Optical and electrical responses to **(A)** mimic pulses, **(B)** mimic pulses and echoes, and **(C)** mimic pulses and series of echoes. Green lines, averaged optical responses recorded by line-scans; red lines, local field potentials (LFPs); blue lines, multiunit activity (MUA). The time delay of the echo was 8 ms. **(D)** Sound level dependence of the averaged calcium responses.

6.3 Results

6.3.1 *Optical and electrical responses evoked by mimic pulses and echoes*

The results of the simultaneous recordings of $\Delta F/F$, LFP, and MUA that were obtained by changing the number of echoes to 0, 1, and 5 are shown in Fig. 6.2. Changes in the LFPs (red lines) and MUAs (blue lines) were recorded, and the changes in the number of peaks corresponding to the number of pulses and echoes were determine. However, the changes in the calcium responses did not follow the number of stimuli. In contrast, as the number of echoes increased, the peak values of $\Delta F/F$ became larger (Fig. 6.2D). Even when the pulse and echo time interval were changed, the results were similar: the $\Delta F/F$ waveforms did not differ, except for the changes in amplitude and peak latency (Fig. 6.3). These results showed that, even with the pseudo pulse and echo sounds, the calcium responses did not follow the electrical activities within milliseconds.
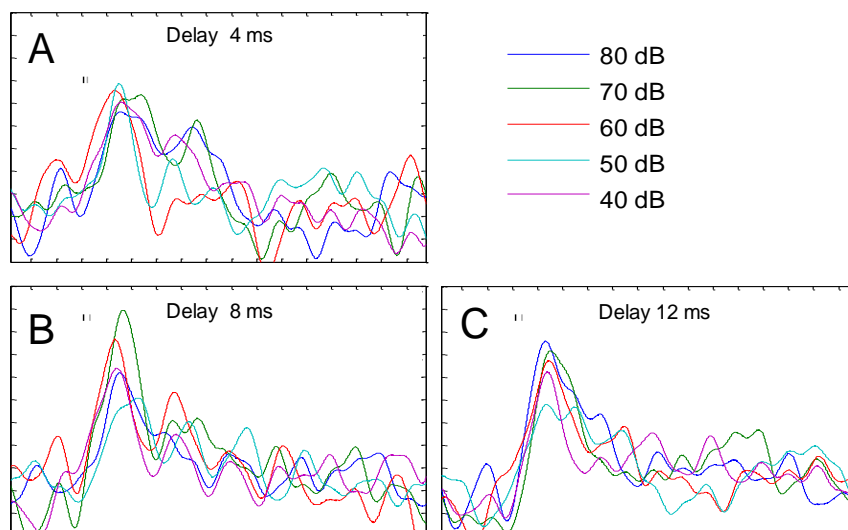
Figure 6.3 Calcium responses to mimic pulses and echoes
(A) Time course of the calcium responses to mimic pulses and echoes. Time delay 4, **(B)** 8, and **(C)** 12 ms. Black and gray bar show the pulses and echoes.
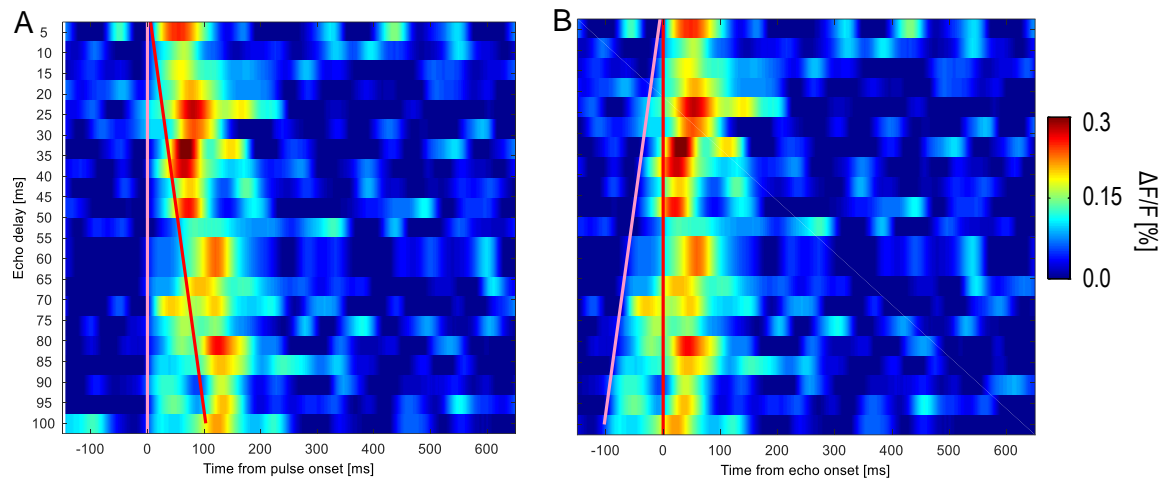
Figure 6.4 Temporal separability of the calcium responses
(A), (B) Heat maps of the calcium responses to mimic pulses and echoes. The time delays between the pulses and echoes were changed from 5 to 100 ms in 5-ms steps. The pink and red lines indicate the onset of the sound stimuli (pulse onset, pink lines; echo onset, red lines).

6.3.2 *Temporal separation of the calcium response*

Because the temporal separation of *ΔF/F* could not be confirmed when the time intervals between the pulses and echoes were on the order of milliseconds, we examined how much of a time difference was needed to separate the calcium responses by systematically changing the time differences between the pulses and echoes. Fig. 6.4 shows waterfall heat maps of the calcium responses, and Fig. 6.5 shows waterfall plots of the LFPs and MUAs. These responses were evoked by changes in the time differences between the pulses and echoes of 5–100 ms in 5-ms steps. In Fig. 6.4, the pink and red lines show the onset of the sound stimuli (pulse onset: pink line; echo onset: red line). The echo onsets (red line) were adjusted to be at 0 ms in Fig. 6.4B.

Comparisons of the electrical activities and calcium responses showed that the bimodalities of the wave could be confirmed with LFP and MUA when the time difference was longer than 10 ms. However, the bimodality of *ΔF/F* was confirmed only when the time delay was 70 ms or more. These results suggest that it is difficult to observe CSN activities as calcium changes.
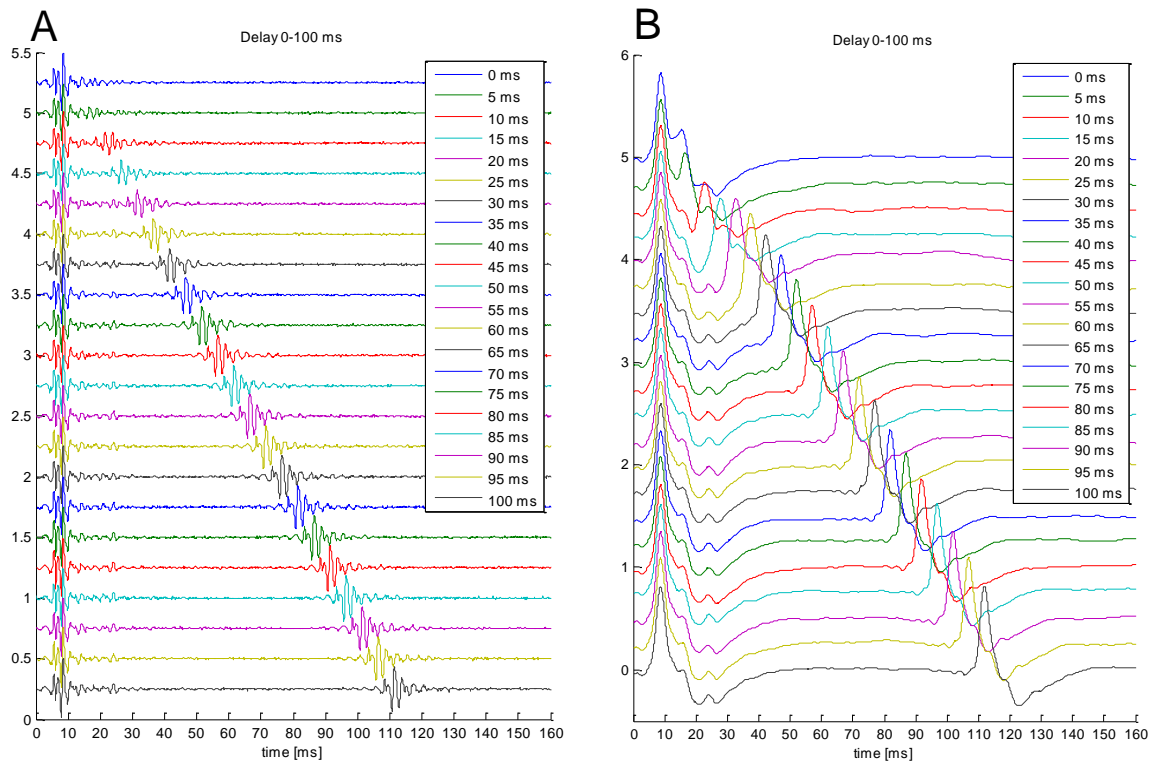
Figure 6.5 Multiunit activity (MUA) and local field potentials (LFPs) in response to mimic pulses and echoes
(A) Waterfall plot of MUA and **(B)** LFPs in response to mimic pulses and echoes. The time delay between the pulse and echo was changed from 5 to 100 ms in 5-ms steps.

6.4 Discussion

When the number of pulses and echoes were increased, the peak amplitude values of the calcium responses increased. This result was thought to be because of the overlap of the calcium responses as a result of an increase in the number of spikes. The results described above, which were in agreement with *in vitro* experimental results (Ikegaya et al., 2005), were thought to reflect the same mechanisms as those underlying the increase in the calcium responses according to the sound duration, as discussed in Chapter 5. These results suggested that it was difficult to distinguish the calcium responses for a long sound stimulus and for multiple consecutive sound stimuli.
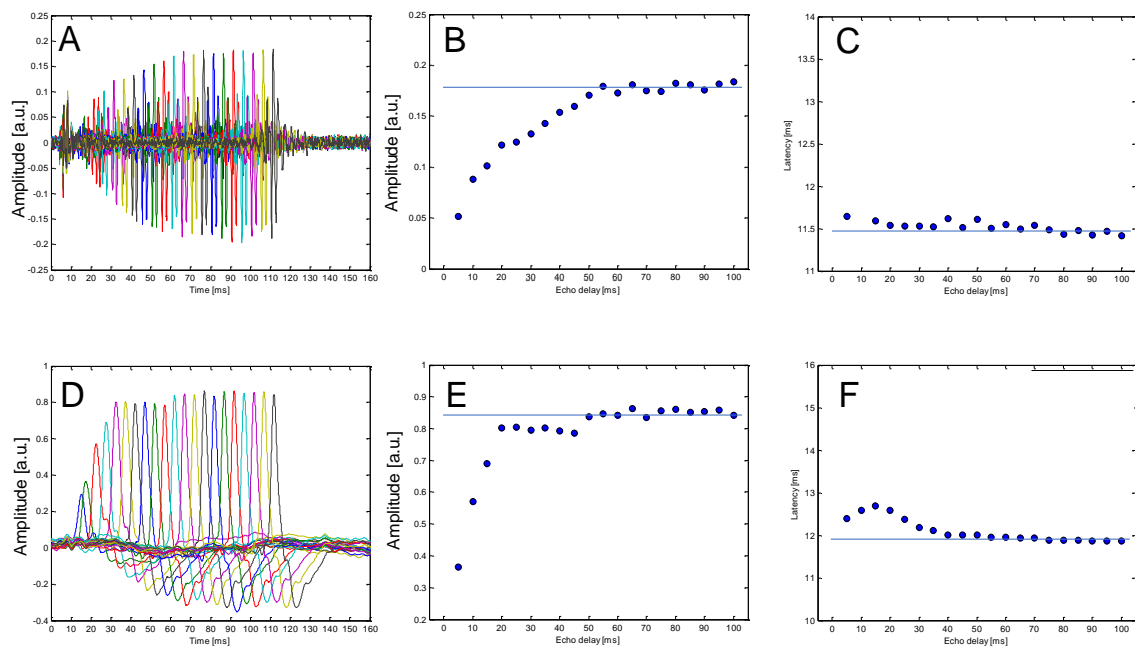
**Figure 6.6 Multiunit activity (MUA) and local field potentials (LFPs) in response to mimic echoes**
(A) MUA and **(D)** LFPs, after subtracting the responses to mimic pulses from the MUAs and LFPs in Fig. 6.5. **(B)** Amplitude-delay function of MUAs and **(E)** LFPs. **(C)** Latency-delay function of MUAs and **(F)** LFPs.

76

As described above, the calcium responses were not separated unless the time interval was 70 ms or longer. In contrast, the LFP and MUA were separated if there was an interval of 10 ms or more. However, the amplitude of the separated waveform was smaller and required a longer time difference to regain the same amplitude as the original one (Fig. 6.5). We subsequently extracted only the responses to the echo sounds by subtracting the responses to the single pulse alone from the those for the LFPs and MUAs (Figs. 6.6A and D). As a result, the amplitudes and peak latencies of the LFPs and MUAs required 50 to 60 ms to regain the original amplitude or peak latency. These results were thought to reflect the influence of slow inhibition in the IC (Covey et al., 1996). Even the calcium response needed more than 70 ms to separate the responses. However, the latency seemed to change with a cycle of 50 ms, as shown in Fig. 6.4B. In Fig. 6.7, the measured peak latencies of $\Delta F/F$ were plotted, which showed that it changed with a cycle of approximately 50 ms. These results suggested that the calcium responses might be influenced by the slow inhibition in the IC and that the time interval required to separate of calcium response might be elongated. In addition, these results showed that it is difficult to measure auditory responses at echo locations, such as the CSN, only with the calcium response.
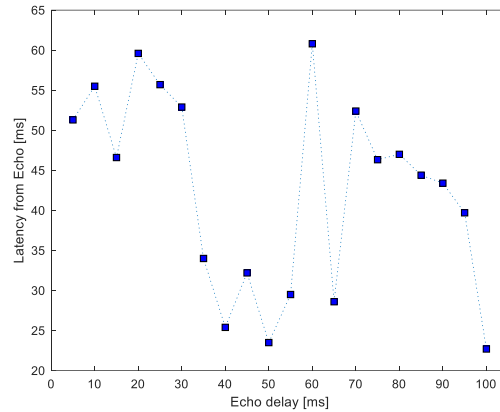
Figure 6.7 Latencies of the calcium responses to mimic echoes
The latency-delay function of *ΔF/F*.

6.5 Summary

We used high speed scanning to optically and electrophysiologically record the auditory responses in the bat IC to pseudo pulses and echo sounds. As a result, electrical activities that corresponded to the pulse and echo sounds were confirmed using LFPs and MUA, respectively. However, the calcium responses did not show separated responses to each sound stimulus. Therefore, we elongated the time interval between the pulses and echoes to examine how long the time differences needed to be to separate the calcium responses. As a result, the calcium responses were separated by time differences of 70 ms or more. Consequently, these results showed that it was difficult to spatially record the optical responses during echolocation with the calcium response alone.

CHAPTER 7. Conclusions

This dissertation discusses that the micro-endoscope was developed to establish a method for measuring auditory responses and that the experimental method was improved while the experiments were conducted using mice and bats.

In this chapter, we summarize the main results of the dissertation, review its contributions, and discuss the future directions of the research.

7.1 Summaries of main results

A. Micro-endoscopy for optical recordings in deep brain areas (Chapter 2)

In Chapter 2, the micro-endoscope was described. The micro-endoscope consists of the combination of a fluorescent microscope, laser scanner, and optical fiber bundle. By inserting an end of the optical fiber bundle into the brain and scanning the surface of the other end, imaging of the deep brain is possible. The optical fiber bundle used had a diameter of 215 μm (or 300 μm) and consisted of 3,000 (6,000) optical single-mode fibers. The end of the bundle that was to be inserted into the brain was an endoscope tip that was polished to a cone shape to minimize its invasiveness. Optical measurements using the micro-endoscope were performed on mice who had been injected with a calcium-sensitive fluorescent dye. As a result, comparisons of the *in vivo* micro-endoscopic images and *in vitro* microscopic images of brain slices that were measured with an epi-fluorescent microscope showed that the endoscopic images had a level of spatial resolution that was sufficient for the detection of each cell body.

In addition, because the tip of the fiber bundle was polished into a cone shape, there was considerable distortion in the spatial domain because of the tip shape. For clear representation of this spatial distortion, we used transgenic mice with yellow fluorescent protein-labeled cells and examined the IC circuits using our micro-endoscope. These results showed that the distances between the cells located in the closer polar angle did not change much with probe advancement, whereas the distances between the cells located with larger polar angle differences were considerably elongated. Although the results on the distances between the cells require careful interpretation, these results indicated that the detection and distinguishing of each cell body was possible in micro-endoscopic images.

B. Optical and electrical responses recorded from the mouse IC (Chapter 3)

In Chapter 3, we describe the measurements of the neural activity in the mouse IC that were performed with the micro-endoscope to optically and electrophysiologically measure auditory responses We processed the endoscopic tip of the optical fiber bundle to use as an electrode. The tip was coated with gold and enamel so that electrophysiological measurements could be performed simultaneously with the optical measurements. We measured the auditory responses that were evoked in the mouse IC by WN and tone bursts and compared the SPL-dependent changes in the electrophysiological responses (LFPs and MUAs) with that of the calcium fluorescence changes ($\Delta F/F$). There were a number of hot spots, which consisted of calcium fluorescence changes that were evoked by sound stimuli. Although we could not determine if these spots were IC neurons because the cell bodies were not labeled,

their size (10–30 μm in diameter) corresponded to the size of the IC neurons (5–30 μm). We subsequently systematically changed the recording depths (150, 500, and 1,500 μm from the brain surface) while recording the calcium responses to tone bursts at varying frequencies (5, 7, 10, 15, 20, 30, 40, and 60 kHz) and SPLs (25–95 dB SPL at 10-dB steps). The frequency-dependent changes of the calcium response were also confirmed by changing the measurement depth. Thus, these results showed that calcium fluorescence changes and electrophysiological activities can be simultaneously measured. As described above, the results of the studies described in this section showed the usefulness of the micro-endoscope.

C. Auditory responses recorded optically in echolocating bats (Chapter 4)

In Chapter 4, the performance of the calcium imaging to establish an optical measurement method using bats as subjects is described. The experimental procedures established with mice were applied to bats, and the optical measurement experiments were performed with the micro-endoscope. The short-tailed fruit bat (C. perspicillata) was used as the subject, and the fluorescence changes induced by the auditory responses evoked by WN bursts and FM sweep sounds were recorded. Depending on the type of sound stimulus, the SPL-dependent changes also differed. The maximum value of the optical response to WN was recorded at 60 dB, whereas that of the response to FM was recorded at 90 dB. In addition, some hot spots with strong changes in fluorescence that corresponded to the size of neurons in the IC of bats were found, which was similar to the findings in the mice experiments. The SPL-dependent changes in the calcium response to each sound stimulus were also investigated. The

results showed that the SPLs that induced strong responses were slightly different, even though the SPL-dependent changes in the mean values over the entire viewfield and the SPL-dependent changes at each hot spot were almost the same. As described above, the results of this study showed that calcium imaging was possible in bats as well as in mice.

D. Fast optical and electrophysiological recordings (Chapter 5)

In chapter 5, the attempts to improve the temporal resolution of the optical measurements using the micro-endoscope are described. The micro-endoscope used a laser scanner, and 53 ms was required to scan one frame image. Modifications were made to try to shorten the scanning time by limiting the range of the scanned area. The results showed that the time resolution could be increased up to 7,550 lines/s by setting the scanning part to only one line. Using this high-speed scanning method (line-scan), optical measurements and electrophysiological measurements were performed on two species of bats (big brown bat, E. fuscus and short-tailed fruit bat, C. perspicillata). The sound stimuli consisted of WN and two types of FM sweeps and tone bursts, and the calcium responses were recorded by changing the SPL and duration of the sound stimulation. The results showed that the peak latencies of the calcium responses varied depending on the stimulus duration. In addition, the peak latencies hardly changed, and the rising inclination of the calcium responses decreased when the SPLs changed. This method showed that more detailed measurements of the time courses of the calcium responses could be performed with line-scans. Although the spatial resolution of line-scans was worsened to enhance the time resolution, the spatial differences in

the calcium responses were recorded within one scanned line. The calcium responses were subsequently compared with the simultaneously recorded electrophysiological responses (LFP and MUA). The peak latencies of these responses differed greatly between the electrical activities and calcium responses (>60 ms). However, when these correlations were examined, positive correlations were found between LFP and MUA and between LFP and $\Delta F/F$. Therefore, although it is not simple to compare electrical activities and calcium responses, these relationships are expected to be revealed by the simultaneous recordings. As described above, these results suggest that combining optical and electrophysiological recordings can lead to the elucidation of the neuronal networks

E. Optical and electrical responses evoked by mimic pulse and echo sounds (Chapter 6)

In Chapter 6, the use of high speed scanning to optically and electrophysiologically record the auditory responses to mimic pulses and echo sounds is described. Big brown bats were used as the subjects. Pulse sounds that simulated FM sounds were used at the echo location, and echo sounds that attenuated the pulse sounds were used as sound stimuli. While changing the time differences between the pulse sounds and the echo sounds/number of echo sounds, the changes in fluorescence of the auditory responses and the electrophysiological responses were recorded. Responses corresponding to the pulse and echo sounds were confirmed in LFP and MUA, respectively. However, the calcium responses increased as the number of echoes increased, but no separate responses were observed for each sound. Therefore, we prolonged the time intervals

of the pulses and echoes by 5 ms for 0–100 ms and confirmed the amount of difference in the time that was required to separate the calcium response. These results confirmed that the calcium response was separated if the difference was 70 ms or longer, but it was not separated when the time interval was shorter than 70 ms. These results suggested that it may be difficult to spatially record the responses at the time of echolocation with the calcium response alone.

7.2 Future works

- **Introduction of fluorescent protein by genetically modified virus**

In the optical measurements of bats, mutant animals cannot be used because it is difficult to breed the bats. Therefore, captured wild bats were used as the subjects in this study. Therefore, as in this study, it is necessary to use calcium-sensitive fluorescent dyes. However, viral vectors that express fluorescent protein in arbitrary cells has been developed, and several experiments have been conducted on mice and songbirds (Tian et al., 2009; Matsui et al., 2012; Zariwala et al., 2012; Bovetti et al., 2014; Barnstedt et al., 2015; Roberts et al., 2017). Although no studies have been performed on the introduction of fluorescent proteins into bats, an example of transgenesis in bats using lentivirus has been reported (Chen et al., 2013; Zhu et al., 2014). Therefore, these results suggest that it is possible to introduce fluorescent proteins to bats. Future studies should use viral applications of fluorescent proteins to label neurons and distinguish cell subtypes.

- **Optical measurement of fast time response with Voltage sensitive dye**

The problem with calcium imaging is that the time response is slower than the actual membrane potential change (Koester and Sakmann, 2000; Grienberger and Konnerth, 2012). Almost all of the optical measurements currently conducted are calcium imaging, and recording calcium or optical responses of fast neural activities, such as auditory responses, is difficult. Although the optical measurements that were made using a VSD had a fast time response, the signal-to-noise ratio was much lower compared with that of the CSD (Tsien, 1980). In recent years, however, VSDs with strong fluorescent sensitivity have been developed, and their practical applications have been advanced (Miller et al., 2012; Woodford et al., 2015; Miller, 2016; Kulkarni et al., 2017). This VSD showed that strong changes were observed in the fluorescence almost without delay of the actual action potential change. Future research should try to combine this fast-response dye with a high-speed image recording method using our microscopic endoscope to identify the neural ensembles that respond during echolocation or other behaviors.

7.3 Final remarks

This dissertation describes the development of a micro-endoscopic system that enabled recordings of the optical and electrical responses in deep brain regions. Consequently, this micro-endoscopic system could record both optical and electrophysiological (LFPs and MUA) data simultaneously. The spatial resolution of this system was lower than that of two-photon excitation microscopy, but it could record signals in deep areas of the brain,

which are not easily accessible by conventional optical recording methods. The temporal resolution of the optical recordings was improved by reducing the size of the scanned area. These results showed that this endoscopic system was able to record with a resolution of sub-millisecond time. The principal finding of the bat experiments was that the optical calcium responses in the IC had slow time courses of the order of tens of milliseconds whether they were recorded from full video frames in the normal-scan procedure or from line-scans. This timescale differed from the submillisecond time course of the electrophysiological responses recorded in the IC. Therefore, it is unlikely that the calcium responses alone will reveal significant aspects of the auditory representation at the level of the individual biosonar broadcasts and echoes, that is, the calcium responses do not reflect the necessarily fast neural events that are required to account for the encoding of biosonar pulse-echo information in the bat's auditory system. However, the simultaneous recording of the optical responses and LFPs and MUA needs to be performed to examine the relationships between these responses, and the micro-endoscope system described in this dissertation should be a useful tool for *in vivo* neurophysiological studies.

REFERENCES

Bandyopadhyay S, Shamma SA, Kanold PO (2010) Dichotomy of functional organization in the mouse auditory cortex. Nat Neurosci 13:361-368.

Barnstedt O, Keating P, Weissenberger Y, King AJ, Dahmen JC (2015) Functional Microarchitecture of the Mouse Dorsal Inferior Colliculus Revealed through In Vivo Two-Photon Calcium Imaging. J Neurosci 35:10927-10939.

Bathellier B, Ushakova L, Rumpel S (2012) Discrete neocortical dynamics predict behavioral categorization of sounds. Neuron 76:435-449.

Bovetti S, Moretti C, Fellin T (2014) Mapping brain circuit function in vivo using two-photon fluorescence microscopy. Microsc Res Tech 77:492-501.

Cant NB (2005) Projections from the cochlear nuclear complex to the inferior colliculus. The inferior colliculus:115-131.

Chen C, Rodriguez FC, Read HL, Escabi MA (2012) Spectrotemporal sound preferences of neighboring inferior colliculus neurons: implications for local circuitry and processing. Front Neural Circuits 6:62.

Chen Q, Zhu T, Jones G, Zhang J, Sun Y (2013) First knockdown gene expression in bat (Hipposideros armiger) brain mediated by lentivirus. Mol Biotechnol 54:564-571.

Cohen L, Keynes R, Hille B (1968) Light scattering and birefringence changes during nerve activity. Nature 218:438-441.

Cohen L, Hille B, Keynes R (1969) Light scattering and birefringence changes during activity in the electric organ of Electrophorus electricus. The Journal of physiology 203:489-509.

Covey E, Casseday JH (1995) The lower brainstem auditory pathways. In: Hearing by bats, pp 235-295: Springer.

Covey E, Kauer JA, Casseday JH (1996) Whole-cell patch-clamp recording reveals subthreshold sound-evoked postsynaptic currents in the inferior colliculus of awake bats. Journal of Neuroscience 16:3009-3018.

Davis H, Zerlin S (1966) Acoustic relations of the human vertex potential. The Journal of the Acoustical Society of America 39:109-116.

Dear SP, Suga N (1995) Delay-tuned neurons in the midbrain of the big brown bat. Journal of neurophysiology 73:1084-1100.

Denk W, Strickler JH, Webb WW (1990) Two-photon laser scanning fluorescence microscopy. Science 248:73-76.

Doroshkevich A, Naselsky P, Verkhodanov OV, Novikov D, Turchaninov V, Novikov I, Christensen P, Chiang L-Y (2005) Gauss–Legendre sky pixelization (GLESP) for CMB maps. International Journal of Modern Physics D 14:275-290.

Durrant JD, Lovrinic JH (1995a) Physiological acoustics of the auditory periphery. In: Bases of Hearing Science, pp 138-195. Baltimore, Md.: Lippincott Williams & Wilkins.

Durrant JD, Lovrinic JH (1995b) Neurophysiology of the auditory system. In: Bases of Hearing Science, pp 196-255. Baltimore, Md.: Lippincott Williams & Wilkins.

Ehret G, Moffat AJ (1985) Inferior colliculus of the house mouse. Journal of Comparative Physiology A: Neuroethology, Sensory, Neural, and Behavioral Physiology 156:619-635.

Feng AS, Simmons JA, Kick SA (1978) Echo detection and target-ranging neurons in the auditory system of the bat Eptesicus fuscus. Science 202:645-648.

Fitzpatrick DC, Kanwal JS, Butman JA, Suga N (1993) Combination-sensitive neurons in the primary auditory cortex of the mustached bat. Journal of Neuroscience 13:931-940.

Flusberg BA, Cocker ED, Piyawattanametha W, Jung JC, Cheung EL, Schnitzer MJ (2005) Fiber-optic fluorescence imaging. Nat Methods 2:941-950.

Göbel W, Kerr JN, Nimmerjahn A, Helmchen F (2004) Miniaturized two-photon microscope based on a flexible coherent fiber bundle and a gradient-index lens objective. Optics letters 29:2521-2523.

Goto A, Nakahara I, Yamaguchi T, Kamioka Y, Sumiyama K, Matsuda M, Nakanishi S, Funabiki K (2015) Circuit-dependent striatal PKA and ERK signaling underlies rapid behavioral shift in mating reaction of male mice. Proc Natl Acad Sci U S A 112:6718-6723.

Goto K, Hiryu S, Riquimaroux H (2010) Frequency tuning and latency organization of responses in the inferior colliculus of Japanese house bat, Pipistrellus abramus a. The Journal of the Acoustical Society of America 128:1452-1459.

Grewe BF, Helmchen F (2009) Optical probing of neuronal ensemble activity. Curr Opin Neurobiol 19:520-529.

Grienberger C, Konnerth A (2012) Imaging calcium in neurons. Neuron 73:862-885.

Grienberger C, Adelsberger H, Stroh A, Milos RI, Garaschuk O, Schierloh A, Nelken I, Konnerth A (2012) Sound-evoked network calcium transients in mouse auditory cortex in vivo. J Physiol 590:899-918.

Griffin DR (1958) Listening in the dark: the acoustic orientation of bats and men.

Hamel EJ, Grewe BF, Parker JG, Schnitzer MJ (2015) Cellular level brain imaging in behaving mammals: an engineering approach. Neuron 86:140-159.

Hayashi Y, Tagawa Y, Yawata S, Nakanishi S, Funabiki K (2012) Spatio-temporal control of neural activity in vivo using fluorescence microendoscopy. Eur J Neurosci 36:2722-2732.

Helmchen F, Denk W (2005) Deep tissue two-photon microscopy. Nat Methods 2:932-940.

Horton NG, Wang K, Kobat D, Clark CG, Wise FW, Schaffer CB, Xu C (2013) In vivo three-photon microscopy of subcortical structures within an intact mouse brain. Nat Photonics 7.

Ikegaya Y, Le Bon-Jego M, Yuste R (2005) Large-scale imaging of cortical network activity with calcium indicators. Neurosci Res 52:132-138.

Issa JB, Haeffele BD, Agarwal A, Bergles DE, Young ED, Yue DT (2014) Multiscale optical Ca2+ imaging of tonal organization in mouse auditory cortex. Neuron 83:944-959.

Ito T, Oliver DL (2012) The basic circuit of the IC: tectothalamic neurons with different patterns of synaptic organization send different messages to the thalamus. Frontiers in neural circuits 6.

Ito T, Hirose J, Murase K, Ikeda H (2014) Determining auditory-evoked activities from multiple cells in layer 1 of the dorsal cortex of the inferior colliculus of mice by in vivo calcium imaging. Brain Res 1590:45-55.

Kajikawa Y, Schroeder CE (2011) How local is the local field potential? Neuron 72:847-858.

Kamioka Y, Sumiyama K, Mizuno R, Sakai Y, Hirata E, Kiyokawa E, Matsuda M (2012) Live imaging of protein kinase activities in transgenic mice expressing FRET biosensors. Cell structure and function 37:65-73.

Kellogg WN, Kohler R (1952) Reactions of the porpoise to ultrasonic frequencies. Science 116:250-252.

Ketten DR (1997) Structure and function in whale ears. Bioacoustics 8:103-135.

Klug A, Khan A, Burger RM, Bauer EE, Hurley LM, Yang L, Grothe B, Halvorsen MB, Park TJ (2000) Latency as a function of intensity in auditory neurons: influences of central processing. Hearing research 148:107-123.

Knudsen EI, Konishi M (1978) Center-surround organization of auditory receptive fields in the owl. Science 202:778-780.

Koester HJ, Sakmann B (2000) Calcium dynamics associated with action potentials in single nerve terminals of pyramidal cells in layer 2/3 of the young rat neocortex. The Journal of physiology 529:625-646.

Kulkarni RU, Kramer DJ, Pourmandi N, Karbasi K, Bateup HS, Miller EW (2017) Voltage-sensitive rhodol with enhanced two-photon brightness. Proc Natl Acad Sci U S A 114:2813-2818.

Leybaert L, de Meyer A, Mabilde C, Sanderson M (2005) A simple and practical method to acquire geometrically correct images with resonant scanning-based line scanning in a custom-built video-rate laser scanning microscope. Journal of microscopy 219:133-140.

Looger LL, Griesbeck O (2012) Genetically encoded neural activity indicators. Current opinion in neurobiology 22:18-23.

Mank M, Santos AF, Direnberger S, Mrsic-Flogel TD, Hofer SB, Stein V, Hendel T, Reiff DF, Levelt C, Borst A, Bonhoeffer T, Hubener M, Griesbeck O (2008) A genetically encoded calcium indicator for chronic in vivo two-photon imaging. Nat Methods 5:805-811.

Matsui R, Tanabe Y, Watanabe D (2012) Avian adeno-associated virus vector efficiently transduces neurons in the embryonic and post-embryonic chicken brain. PLoS One 7:e48730.

91

Meininger V, Pol D, Derer P (1986) The inferior colliculus of the mouse. A Nissl and
    Golgi study. Neuroscience 17:1159-1179.

Melcher JR, Kiang NY (1996) Generators of the brainstem auditory evoked potential in
    cat III: identified cell populations. Hearing research 93:52-71.

Melcher JR, Guinan JJ, Knudson IM, Kiang NY (1996) Generators of the brainstem
    auditory evoked potential in cat. II. Correlating lesion sites with waveform
    changes. Hearing research 93:28-51.

Miller EW (2016) Small molecule fluorescent voltage indicators for studying membrane
    potential. Curr Opin Chem Biol 33:74-80.

Miller EW, Lin JY, Frady EP, Steinbach PA, Kristan WB, Jr., Tsien RY (2012) Optically
    monitoring voltage in neurons by photo-induced electron transfer through
    molecular wires. Proc Natl Acad Sci U S A 109:2114-2119.

Miyamoto D, Murayama M (2016) The fiber-optic imaging and manipulation of neural
    activity during animal behavior. Neurosci Res 103:1-9.

Miyawaki A, Llopis J, Heim R, McCaffery JM, Adams JA, Ikura M, Tsien RY (1997)
    Fluorescent indicators for Ca2+ based on green fluorescent proteins and
    calmodulin. Nature 388:882-887.

Murayama M, Larkum ME (2009) In vivo dendritic calcium imaging with a fiberoptic
    periscope system. Nat Protoc 4:1551-1559.

Murayama M, Perez-Garci E, Luscher HR, Larkum ME (2007) Fiberoptic system for
    recording dendritic calcium signals in layer 5 neocortical pyramidal cells in
    freely moving rats. J Neurophysiol 98:1791-1805.

Nakamura O (1999) Fundamental of two-photon microscopy. Microscopy research and
    technique 47:165-171.

Neuweiler G (2000a) Diet, digestion, and energy balance. In: The biology of bats, pp
    98-116: Oxford University Press on Demand.

Neuweiler G (2000b) Echolocation. In: The biology of bats, pp 140-209: Oxford University Press on Demand.

O'Neill WE, Suga N (1979) Target range-sensitive neurons in the auditory cortex of the mustache bat. Science 203:69-73.

Oliver DL (2005) Neuronal organization in the inferior colliculus. In: The inferior colliculus, pp 69-114: Springer.

Olsen JF, Suga N (1991) Combination-sensitive neurons in the medial geniculate body of the mustached bat: encoding of relative velocity information. Journal of neurophysiology 65:1254-1274.

Onishi S, Davis H (1968) Effects of duration and rise time of tone bursts on evoked V potentials. The Journal of the Acoustical Society of America 44:582-591.

Osanai M, Suzuki T, Tamura A, Yonemura T, Mori I, Yanagawa Y, Yawo H, Mushiake H (2013) Development of a micro-imaging probe for functional brain imaging. Neurosci Res 75:46-52.

Ozbay BN, Losacco JT, Cormack R, Weir R, Bright VM, Gopinath JT, Restrepo D, Gibson EA (2015) Miniaturized fiber-coupled confocal fluorescence microscope with an electrowetting variable focus lens using no moving parts. Opt Lett 40:2553-2556.

Paredes RM, Etzler JC, Watts LT, Zheng W, Lechleiter JD (2008) Chemical calcium indicators. Methods 46:143-151.

Parkkonen L, Fujiki N, Mäkelä JP (2009) Sources of auditory brainstem responses revisited: contribution by magnetoencephalography. Human brain mapping 30:1772-1782.

Pedemonte M, Torterolo P, Velluti RA (1997) In vivo intracellular characteristics of inferior colliculus neurons in guinea pigs. Brain research 759:24-31.

Pena JL, Viete S, Funabiki K, Saberi K, Konishi M (2001) Cochlear and neural delays for coincidence detection in owls. Journal of Neuroscience 21:9455-9459.

Perchant A, Le Goualher G, Genet M, Viellerobe B, Berier K (2004) An integrated fibered confocal microscopy system for in vivo and in situ fluorescence imaging-applications to endoscopy in small animal imaging. In: Biomedical Imaging: Nano to Macro, 2004. IEEE International Symposium on, pp 692-695: IEEE.

Peterka DS, Takahashi H, Yuste R (2011) Imaging voltage in neurons. Neuron 69:9-21.

Phillips D, Hall S, Guo Y, Burkard R (2001) Sensitivity of unanesthetized chinchilla auditory system to noise burst onset, and the effects of carboplatin. Hearing research 155:133-142.

Pierce GW, Griffin DR (1938) Experimental Determination of Supersonic Notes Emitted by Bats. Journal of Mammalogy 19:454-455.

Portfors CV, Mayko ZM, Jonson K, Cha GF, Roberts PD (2011) Spatial organization of receptive fields in the auditory midbrain of awake mouse. Neuroscience 193:429-439.

Rees A, Møller AR (1983) Responses of neurons in the inferior colliculus of the rat to AM and FM tones. Hearing research 10:301-330.

Rees A, Palmer AR (1988) Rate-intensity functions and their modification by broadband noise for neurons in the guinea pig inferior colliculus. The Journal of the Acoustical Society of America 83:1488-1498.

Rees A, Sarbaz A, Malmierca MS, Le Beau FE (1997) Regularity of firing of neurons in the inferior colliculus. Journal of neurophysiology 77:2945-2965.

Roberts TF, Hisey E, Tanaka M, Kearney MG, Chattree G, Yang CF, Shah NM, Mooney R (2017) Identification of a motor-to-auditory pathway important for vocal learning. Nat Neurosci 20:978-986.

Rochefort NL, Jia H, Konnerth A (2008) Calcium imaging in the living brain: prospects for molecular medicine. Trends Mol Med 14:389-399.

Sandison DR, Webb WW (1994) Background rejection and signal-to-noise optimization in confocal and alternative fluorescence microscopes. Applied optics 33:603-615.

Schevill WE, McBride AF (1956) Evidence for echolocation by cetaceans. Deep-sea research (1953) 3:153-154.

Schofield BR (2005) Superior olivary complex and lateral lemniscal connections of the auditory midbrain. The inferior colliculus:132-154.

Schreiner CE, Langner G (1997) Laminar fine structure of frequency organization in auditory midbrain. Nature 388:383-386.

Schuller G, O'neill W, Radtke-Schuller S (1991) Facilitation and Delay Sensitivity of Auditory Cortex Neurons in CF-FM Bats, Rhinolophus rouxi and Pteronotus p. parnellii. European Journal of Neuroscience 3:1165-1181.

Schulz K, Sydekum E, Krueppel R, Engelbrecht CJ, Schlegel F, Schroter A, Rudin M, Helmchen F (2012) Simultaneous BOLD fMRI and fiber-optic calcium recording in rat neocortex. Nat Methods 9:597-602.

Simmons JA (2012) Bats use a neuronally implemented computational acoustic model to form sonar images. Curr Opin Neurobiol 22:311-319.

Simmons JA, Ferragamo MJ, Saillant PA, Haresign T, Wotton JM, Dear SP, Lee DN (1995) Auditory Dimensions of Acoustic Images in Echolocation. In: Hearing by Bats, pp 146-190.

Starr A, Hamilton A (1976) Correlation between confirmed sites of neurological lesions and abnormalities of far-field auditory brainstem responses. Electroencephalography and clinical neurophysiology 41:595.

Stiebler I, Ehret G (1985) Inferior colliculus of the house mouse. I. A quantitative study of tonotopic organization, frequency representation, and tone-threshold distribution. Journal of Comparative Neurology 238:65-76.

Suga N (2015) Neural processing of auditory signals in the time domain: delay-tuned coincidence detectors in the mustached bat. Hear Res 324:19-36.

Suga N, O'Neill WE, Manabe T (1978) Cortical neurons sensitive to combinations of information-bearing elements of biosonar signals in the mustache bat. Science 200:778-781.

Suga N, O'Neill WE, Kujirai K, Manabe T (1983) Specificity of combination-sensitive neurons for processing of complex biosonar signals in auditory cortex of the mustached bat. Journal of Neurophysiology.

Sullivan MR, Nimmerjahn A, Sarkisov DV, Helmchen F, Wang SS-H (2005) In vivo calcium imaging of circuit activity in cerebellar cortex. Journal of neurophysiology 94:1636-1644.

Sullivan WE (1982) Neural representation of target distance in auditory cortex of the echolocating bat Myotis lucifugus. Journal of Neurophysiology 48:1011-1032.

Tasaki I, Watanabe A, Sandlin R, Carnay L (1968) Changes in fluorescence, turbidity, and birefringence associated with nerve excitation. Proc Natl Acad Sci U S A 61:883-888.

Thaler L, Goodale MA (2016) Echolocation in humans: an overview. Wiley Interdiscip Rev Cogn Sci 7:382-393.

Tian L, Hires SA, Mao T, Huber D, Chiappe ME, Chalasani SH, Petreanu L, Akerboom J, McKinney SA, Schreiter ER, Bargmann CI, Jayaraman V, Svoboda K, Looger LL (2009) Imaging neural activity in worms, flies and mice with improved GCaMP calcium indicators. Nat Methods 6:875-881.

Tsien RY (1980) New calcium indicators and buffers with high selectivity against magnesium and protons: design, synthesis, and properties of prototype structures. Biochemistry 19:2396-2404.

Tsien RY (1981) A non-disruptive technique for loading calcium buffers and indicators into cells. Nature 290:527-528.

Vincent P, Maskos U, Charvet I, Bourgeais L, Stoppini L, Leresche N, Changeux JP, Lambert R, Meda P, Paupardin-Tritsch D (2006) Live imaging of neural structure and function by fibred fluorescence microscopy. EMBO Rep 7:1154-1161.

Wenstrup JJ (2005) The tectothalamic system. In: The inferior colliculus, pp 200-230: Springer.

Wenstrup JJ, Nataraj K, Sanchez JT (2012) Mechanisms of spectral and temporal integration in the mustached bat inferior colliculus. Front Neural Circuits 6:75.

Woodford CR, Frady EP, Smith RS, Morey B, Canzi G, Palida SF, Araneda RC, Kristan WB, Jr., Kubiak CP, Miller EW, Tsien RY (2015) Improved PeT molecules for optically sensing voltage in neurons. J Am Chem Soc 137:1817-1824.

Yashiro H, Nakahara I, Funabiki K, Riquimaroux H (2017a) Micro-endoscopic system for functional assessment of neural circuits in deep brain regions: Simultaneous optical and electrical recordings of auditory responses in mouse's inferior colliculus. Neurosci Res 119:61-69.

Yashiro H, Funabiki K, Simmons AM, Simmons JA, Riquimaroux H (2017b) Functional optical imaging from bat inferior colliculus using a micro-endoscope. Proc Mtgs Acoust 29.

Zariwala HA, Borghuis BG, Hoogland TM, Madisen L, Tian L, De Zeeuw CI, Zeng H, Looger LL, Svoboda K, Chen TW (2012) A Cre-dependent GCaMP3 reporter mouse for neuronal imaging in vivo. J Neurosci 32:3131-3141.

Zhu T, Yuan L, Jones G, Hua P, He G, Chen J, Zhang S (2014) OB-RL silencing inhibits the thermoregulatory ability of Great Roundleaf Bats (Hipposideros armiger). Gen Comp Endocrinol 204:80-87.

Ziv Y, Ghosh KK (2015) Miniature microscopes for large-scale imaging of neuronal activity in freely behaving rodents. Curr Opin Neurobiol 32:141-147.

CURRICULUM VITAE

Hidetaka Yashiro

Education:

M.Sc., Engineering, Doshisha University, Kyotanabe, Kyoto, Japan, 2015

B.Sc, Engineering, Doshisha University, Kyotanabe, Kyoto, Japan, 2013

Awards:

The Student Presentation Award, Acoustical Society of Japan, 2014

○H. Iwabayashi, **H. Yashiro**, K. I. Kobayasi, H. Riquimaroux, "Vocalizing system in Mongolian gerbil (*Meriones unguiculatus*): mutilation of inferior laryngeal nerves"

Grants and Fellowships:

Doshisha University Reduced-Tuition Scholarships (2013)

Research Fellowships of Japan Society for the Promotion of Science for Young Scientists (DC1) (04/2015-03/2018)

November 2017